sustainability

MDPI

Review

Topological Advances in Isolated DC–DC Converters: High-Efficiency Design for Renewable Energy Integration

Sergio Coelho *, Vitor Monteiro and Joao L. Afonso

ALGORITMI Research Centre/LASI, Department of Industrial Electronics, University of Minho, 4800-058 Guimaraes, Portugal; vmonteiro@dei.uminho.pt (V.M.); jla@dei.uminho.pt (J.L.A.)
* Correspondence: sergio.coelho@algoritmi.uminho.pt

Abstract: The increasing penetration of renewable energy sources (RESs) into medium-voltage (MV) and low-voltage (LV) power systems presents significant challenges in ensuring power grid stability and energy sustainability. Advanced power conversion technologies are essential to mitigate voltage and frequency fluctuations while meeting stringent power quality standards. RES-based generation systems typically employ multistage power electronics to achieve: (i) maximum power point tracking; (ii) galvanic isolation and voltage transformation; (iii) high-quality power injection into the power grid. In this context, this paper provides a comprehensive review of up-to-date isolated DC–DC converter topologies tailored for the integration of RES. As a contribution to support this topic, recent advancements in solid-state transformers (SSTs) are explored, with particular emphasis on the adoption of wide bandgap (WBG) semiconductors technologies, such as silicon carbide (SiC) and gallium nitride (GaN). These devices have revolutionized modern power systems by enabling operation at a higher switching frequency, enhanced efficiency, and increased power density. By consolidating state-of-the-art advancements and identifying technical challenges, this review offers insights into the suitability of power converter topologies in light of future trends, serving as a valuable resource for optimizing grid-connected RES-based sustainable power systems.

Keywords: renewable energy; isolated DC–DC converter; solid-state transformer; high-frequency transformer; sustainable development

Academic Editor: Jack Barkenbus

Received: 30 December 2024
Revised: 27 February 2025
Accepted: 4 March 2025
Published: 7 March 2025

Citation: Coelho, S.; Monteiro, V.; Afonso, J.L. Topological Advances in Isolated DC–DC Converters: High-Efficiency Design for Renewable Energy Integration. *Sustainability* **2025**, *17*, 2336. https://doi.org/10.3390/su17062336

1. Introduction

Environmental sustainability is widely recognized as a critical concern across diverse technological domains. Achieving carbon neutrality demands innovative solutions that effectively reduce greenhouse gas emissions while simultaneously catalyzing a paradigm shift within the energy sector, encompassing key areas such as generation, transportation, and industrial processes. As reported by the International Energy Agency, the energy sector is responsible for around 85% of total CO_2 emissions. In 2023, energy-related activities contributed to a record high of 37.7 gigatons of CO_2 [1]. Notably, the production of electricity and heat is identified as a major contributor to the above-mentioned emissions [2].

Over the last decades, partly due to growing environmental awareness, electricity production on the basis of renewable energy sources (RESs) has gained greater preponderance in the global energy mix. As reported in [3], the increase in power generation is supported by a surge in wind and solar production, helping to decarbonize the energy sector. Despite the impossibility of completely canceling the emissions of greenhouse gasses, an affirmative response to the inclusion of RES-based systems would significantly

contribute to achieving the objectives proposed in the Paris Agreement, celebrated in 2015 and adopted by 196 countries [4].

In addition to transitioning towards clean energy production, it is equally important to prioritize the advancement of electric mobility [5,6], as well as energy storage, e.g., battery production, charge, and recycling [7]. Increasing the focus on such aspects significantly contributes to improving environmental quality and serves as the foundation for an inevitable and anticipated energy transition.

The field of power electronics plays an important and facilitating role in the integration of energy storage systems ESSs, electric vehicles (EVs), and RES-based systems into the utility grid. The growing propagation of such emerging technologies, most of them natively operating in DC, translates, on the other hand, into a series of challenges for the utility grid since, in the actual mold, its infrastructure and organization do not meet the expected premises [8,9]. Future smart grids settle on the principle of power bidirectionality between energy producers and consumers, which does not occur nowadays. It is vital to implement and develop more intelligent, reliable, and sustainable power grid architectures, abandoning centralized structures and migrating to decentralized ideologies [10].

In view of the increasing spread of emerging power devices, the different types of power quality problems have also increased. In the case of strong integration of RES-based energy generation systems, the main concerns relate to harmonic content and voltage and frequency fluctuations [11]. As expected, considering that the energy production profile is dependent on weather conditions, the stronger the integration of RESs, the greater the variability. Moreover, such a scenario also provokes repercussions on the interface between DC devices and AC distribution lines since voltage transients may occur, the vast majority of which are critical to the operation of the system as a whole.

In line with these challenges, coupled with the increasing difficulty of controlling voltage fluctuations at the point of common coupling (PCC), it is crucial to adopt new fault suppression mechanisms, strategies aimed at enhancing power quality and, fundamentally, suitable power electronics systems tailored to each scenario and RES [12]. While wind and hydropower generation have already reached an advanced stage of technological maturity, solar photovoltaic (PV) energy stands out as the most promising path for the development of new power electronics devices [13]. However, these challenges and corresponding solutions extend to various RESs and should be considered for developing interfacing systems with higher efficiency, flexibility, and added functionalities. Recent research has been conducted to address these needs, focusing on the exploration of new architectures, paradigms, power converter topologies, and modulation techniques.

Besides the conventional functionalities of galvanic isolation and maximum power point tracking (MPPT) control algorithms, innovative RES interfacing systems must also efficiently manage the energy needs of producers and consumers. Among these, in alignment with the concept of the smart grid, the mitigation of power quality problems, fault tolerance mechanisms, and the inclusion of ancillary services, a special feature concerning the dissemination of microgrids in decentralized architectures, are highlighted [14].

In line with the current trends, solid-state transformers (SSTs) stand out for their versatility and flexibility, enabling a galvanically isolated interface between two or more power devices through a high-frequency transformer (HFT) [15]. However, the use of medium-frequency transformers (MFTs) is equally valid, especially in high-power scenarios. Connecting RES-based generation systems to the utility grid is solely one of the several SST applications [16,17]. As with some existing multistage systems, three power stages are considered, each of them correspondingly guaranteeing (i) MPPT; (ii) galvanic isolation and voltage rise; and (iii) power injection into the utility grid. Nonetheless, while acknowledging the importance of each power stage, the intermediate one, traditionally

associated with the isolated DC–DC converter, plays a significant role in the system's operability. Beyond the benefits of incorporating a galvanically isolated converter, e.g., the elimination circulating current paths and improved safety in high-power scenarios, it is pertinent to analyze these features with high-frequency (HF) switching. This approach leads to a significant reduction in the volume and weight of power converters and passive elements, i.e., transformers, inductors, and capacitors.

Given the growing proliferation of RES-based energy generation systems, this review paper presents an overview of the most critical and up-to-date topologies for unidirectional isolated DC–DC power converters. In the literature, some review papers are commonly found about this subject; however, none are as comprehensive as this one [18–23]. The main and distinguished contributions of this paper include the following: (i) a comprehensive review of possible architectures and connection schemes for RES-based systems interfacing with the utility grid; (ii) an extended analysis of the most relevant and recent topologies, focusing on practical implementations rather than a broad, theoretical presentation of designs that are no longer suitable for modern applications; (iii) an in-depth study of phase-shift modulation techniques for bidirectional isolated DC–DC power converters, emphasizing their impact on efficiency and dynamic performance; (iv) a comparative discussion of DC–DC topologies, outlining the key strengths of each topology while associating their classification (conventional low-power, bridge-based, and multilevel converters) with their most conventional application cases; (v) an overview of wide-bandgap (WBG) semiconductors and their role in next-generation power converters, highlighting their advantages in terms of switching speed, thermal performance, and efficiency improvements. Furthermore, the study explores future directions in the field, focusing on the control algorithms, modulation techniques, and fault-tolerant mechanisms that enhance converters' flexibility and resilience.

Thus, this review paper is organized as follows: Section 2 depicts the main architecture schemes for the interfacing system. Section 3 extensively analyzes and describes isolated DC–DC topologies to interface with RES-based generation systems, distinguishing between conventional structures, bridge-based converters, and multilevel topologies. Section 4 provides a comparative study between the previously analyzed DC–DC topologies, highlighting their relevance to the proposed topic. A concise overview of WBG devices is conducted in Section 5, while the main conclusions are outlined in Section 6.

2. Power Electronics Systems for RES-Based Generation Technologies

The integration of RES-based power generation units, which is considered inevitable in future smart grids, should be approached with a focus on favorable economic and social premises [24–26]. Simultaneously, from a technical perspective, it is essential to ensure the energy needs of consumers at all times by implementing smoothing mechanisms to address the intermittent generation profile of RESs. While ESSs are often linked with renewables, their widespread adoption is hindered by challenges such as costs and technological maturity [27]. To achieve this objective, the power converters that interface the utility grid and a specific RES will play a significant role in energy management. Similarly to SSTs, these power converters will incorporate added functionalities. Hence, it is essential to select appropriate power electronics solutions, ensuring that the chosen devices are well suited for the specific application requirements.

The main RES-based energy generation elements can be categorized into solar PV and turbine generator technologies, which encompass, e.g., hydro, wind, and geothermal energy. In rotational systems, the speed of the turbine's central axis can be either fixed or variable. Figure 1 illustrates the four configurations commonly considered: (i) fixed speed; (ii) partial variable speed; (iii) variable speed with a partial-scale frequency converter; and

(iv) variable speed with a full-scale power converter. In variable-speed systems, the use of voltage source converters in a back-to-back arrangement enables the incorporation of MPPT algorithms, reactive power compensation, increased robustness, and an enhanced rotation speed of the generator [28,29].

As previously stated, the use of bulky components and devices, such as low-frequency transformers (LFTs), leads to reduced efficiency ratings, lower reliability, and higher costs. Therefore, the adoption of converters with higher power density, i.e., based on HFTs or MFTs, is seen as the most viable solution. This situation is justified in [30–33], where various isolated interface configurations were introduced for variable-speed wind turbines and high-voltage direct current (HVDC) systems in offshore wind farms. In addition, [34] proposed replacing the common LFT with a SST structure.

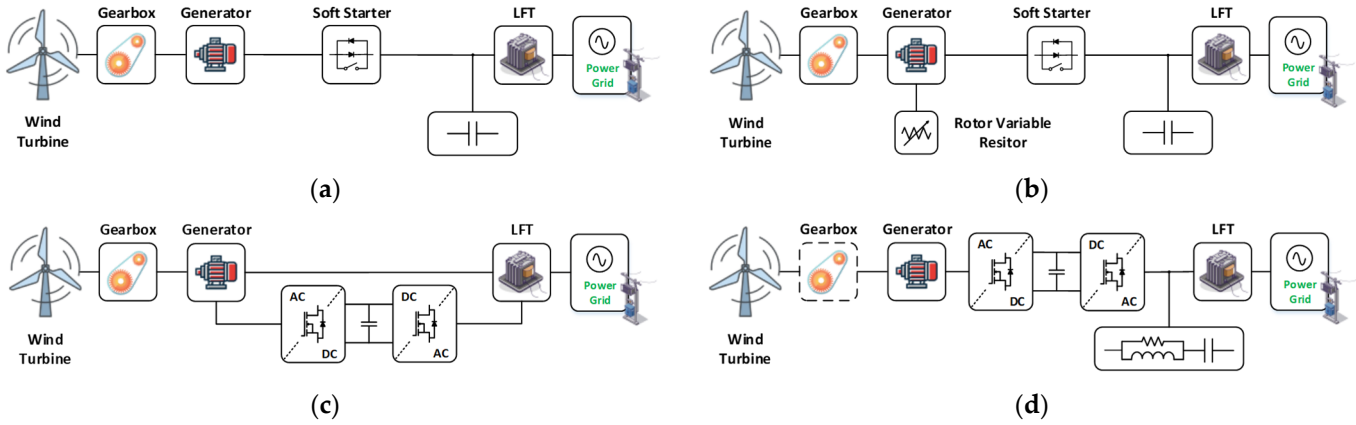

Figure 1. Possible architectures for interfacing turbine generator technologies with the utility grid: (**a**) fixed speed; (**b**) partial variable speed; (**c**) variable speed with partial-scale frequency converter; and (**d**) variable speed with full-scale power converter.

Upon analyzing the literature and recent energy data, it becomes evident that both fuel cells and solar PV technology offer the greatest potential for innovation and evolution. Regarding solar PV, such technological maturation may involve modifications in the characteristics of the modules, but more notably, it necessitates improvements in the interface system between this RES and the utility grid. As observed in Figure 2, depending on the architecture and connection between a certain number of modules, a different number of conversion stages must also be picked [35].

For low-power applications, a single inverting stage may be commonly applied, whereas for a multistring configuration, multistage architectures are always required [36]. This scenario is equally replicable in microinverter configurations, in which a dedicated power converter is associated with each solar PV module. On the other hand, for medium- and high-power scenarios, centralized and multistring configurations are normally considered. Nevertheless, the remaining architectures, albeit less commonly, may be equally used, as proven in [37], where a comparative study regarding power quality, costs, general characteristics, and power losses in large-scale solar PV power plants was carried out. As expected, in higher power scenarios, to reach the desired voltage and current values, several modules must be interconnected. As with microinverter configurations, each solar PV array has a dedicated DC–DC power converter, which consequently, may result in different arrangements for the power converters, i.e., cascade or in parallel. In a single-stage scenario, the converter of each module or array is, necessarily, an inverter, whilst the combination of topologies in a multistage scenario, as seen in Figure 3, provides greater controllability and flexibility to the solar PV system. For these cases, a DC–DC converter is dedicated to each module (with MPPT functionality), and one or more DC–AC converter is used to invert the power generated by all the arrays.

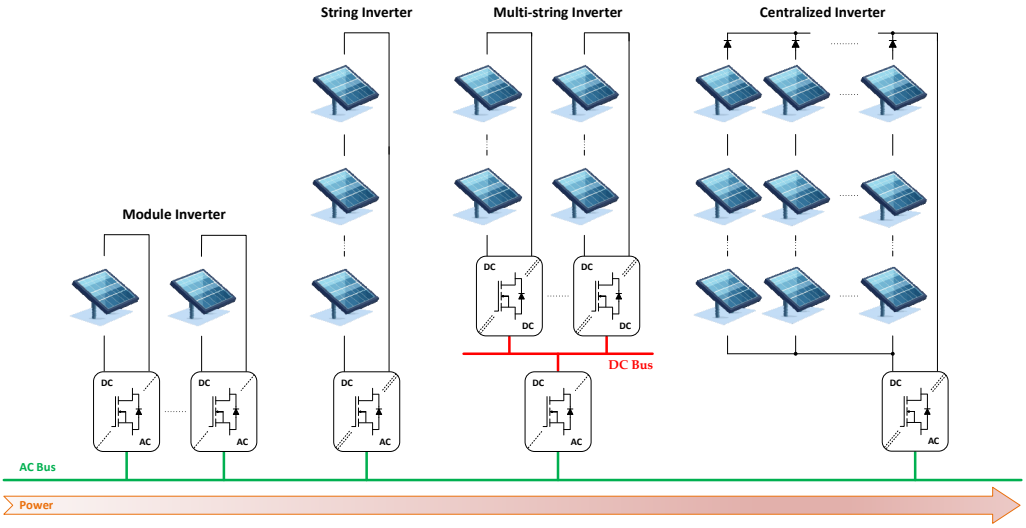

Figure 2. Possible arrangements for grid-connected PV systems: module inverter, string inverter, multistring inverter, and centralized inverter configurations.

For any scenario involving solar PV modules, i.e., residential, commercial, portable, and, most importantly, large-scale power plants, there is always a need for isolation due to safety issues. As already mentioned in the introduction, the inclusion of a galvanically isolated transformer, although not mandatory in certain cases, allows, in addition, the prevention of equipment damage or malfunctioning due to electrical faults (e.g., short circuits). Likewise, the efficiency of solar PV systems becomes, consequently, higher, since possible paths for leakage currents are eliminated.

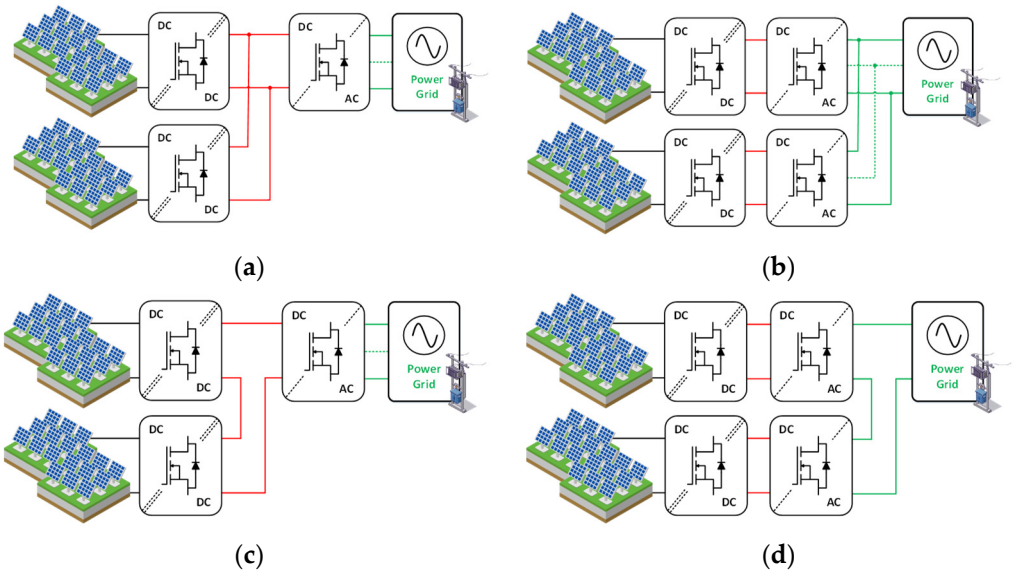

Figure 3. Possible multistage multiple input configurations to interface grid-connected PV systems: (**a**) parallel DC; (**b**) parallel AC; (**c**) cascade DC; and (**d**) cascade AC.

As with solar PV systems, the use of fuel cells also gathers strong consensus within the scientific community as a prominent technological trend with substantial developmental potential. These devices directly convert chemical energy into electrical energy, typically relying on hydrogen as the primary fuel source. This chemical reaction enables the generation of electricity in a clean and efficient manner, although power electronics converters are required to regulate the generated values from each individual cell.

In line with any renewable technology, based on the specific requirements of the system, such converters must be responsible for voltage, current, and, in the case of AC systems, frequency adjustments. However, as experienced with solar PV modules, the output values of a fuel cell will be influenced by temperature fluctuations, load changes, and variations in the fuel supply [38–40]. Therefore, power converters also bear the responsibility of providing stable and reliable operation to the RES-based generation system. This necessitates the implementation of appropriate modulation and control algorithms. Notably, MPPT control algorithms are once again mandatory, with numerous variants commonly documented in the literature, as depicted in [41–44].

Fuel cells, in a simplified manner, can be described as a DC energy source and, as such, are commonly associated with and integrated into multiple input architectures, as depicted in Figure 3. This approach aims to enhance power generation, efficiency, and flexibility. Depending on the application scenario, these DC–DC power converters can also be isolated or non-isolated, as mentioned in [45]. In this comparative study, all possible topologies for interfacing with fuel cells were enumerated, as well as a detailed section regarding technical challenges, power quality problems, and power control issues.

For multiple input systems, careful attention must be devoted to energy management, particularly in hybrid scenarios involving different RESs. Interface systems must adjust various voltage and current values to efficiently deliver energy to the utility grid, loads, or ESSs. To this end, mechanisms for phase and frequency synchronization, management and regulation of imbalances and fluctuations, as well as mitigation and smoothing of transients between different RESs, need to be ensured [46]. Among various examples, power sharing techniques are highlighted, as indicated in [47].

The need for isolation is equally highlighted in turbine generator technologies. Both in this case and in large-scale solar PV power plants, LFTs are used nowadays for interfacing with low-voltage feeders, which confer a static and passive behavior in the face of possible momentary changes in operating conditions. In this regard, for the above-mentioned reasons, migrating towards isolated power electronics solutions switching at medium- or high-frequencies, e.g., the SST (shown in its traditional structure in Figure 4), is seen as one of the facilitating trends for the continuous dissemination of smart grids and microgrids. Furthermore, for any of the cases illustrated in Figures 2–4, the three-phase configuration may also be considered.

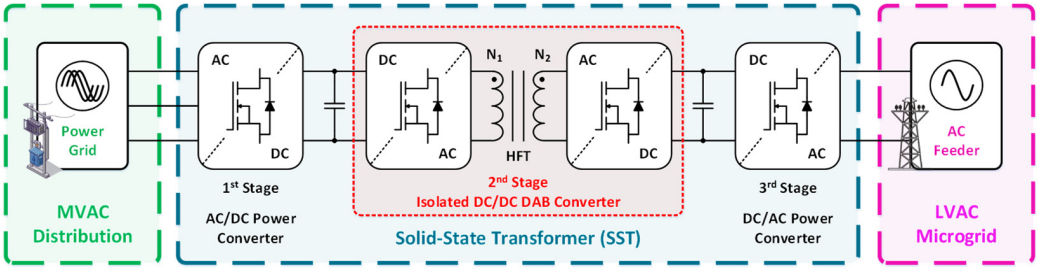

Figure 4. Traditional three-stage structure of a solid-state transformer (SST).

The isolated DC–DC conversion stage, depending on the objectives, may be employed at different points in the interface circuit. For instance, in cases where each module or array disposes of a dedicated converter, isolation can be achieved individually (using multiple converters) or globally, i.e., through a single isolated power converter when interfacing with the utility grid. As expected, the greater the number of isolated power converters used, the greater the cost of the entire installation, but the greater the safety and flexibility. In other words, each array can be sized independently, a particularly useful feature when solar PV modules are subject to different radiation levels or shading. On the other hand, a greater number of isolated power converters also leads to fluctuating efficiency values,

since transformer losses are replicated in multiple points. With regard to reliability, higher values are achieved if each array is isolated from the others since possible localized faults will not represent a reprisal for the global solar PV system.

Due to the growing adoption of emerging DC power devices, the establishment and utilization of DC power grids have become more prevalent. As a key element, such architectures potentially allow for an effective reduction in the number of conversion stages, which consequently translates into enhanced performance and reduced losses. In DC systems, issues related to power quality are also effectively addressed, thereby facilitating the integration of RES-based systems. In the case of DC microgrids, frequency fluctuations are also easily mitigated, which presents a significant advantage during islanding mode.

On the other hand, the migrations towards DC power grids still lack technological maturity and would require a significant overhaul of a substantial portion of the existing infrastructure. Furthermore, the standards and regulatory frameworks for the implementation of such DC structures are still in an unstable phase, precluding their immediate adoption. In addition, DC faults are recognized as one of the major limitations to the ongoing proliferation of DC power grids. In most instances, power converter topologies are chosen based on their capability and characteristics to efficiently mitigate such faults.

According to [48], DC pole-to-pole faults originate from either a short-circuit occurrence or insulation breakdown. Since the impedance of a DC line is much lower when compared to traditional AC systems, this type of fault will result in an almost immediate capacitor discharge. While less common, DC pole-to-pole faults can cause severe damage to electronic equipment, the majority of which have limited capabilities in terms of overcurrent protection. Therefore, a faster response time is required for protection systems, which is considered the primary drawback compared to AC energy transmission and distribution systems [49].

As potential problems caused by DC faults can quickly escalate into a cascade effect, affecting several devices, it is imperative for modern power systems to incorporate advanced monitoring and control technologies. Additionally, robustness and redundancy should also be strengthened to enhance the stability of transmission and distribution systems, thereby isolating DC faults.

To mitigate these issues, DC circuit breakers should be integrated into the DC system. Alternatively, converter topologies with enhanced DC-side fault handling capabilities, such as modular multilevel converters (MMCs) [50], can also be employed. Nonetheless, it is always advisable to use multiple DC circuit breakers to prevent extensive propagation of the fault. As a result, other segments of the DC line can continue to operate redundantly, similar to current AC systems. In turn, when utilizing power converters as an active fault mitigation element, appropriate control algorithms should also be considered, as demonstrated in [51]. In this article, fault behaviors in the modal-domain, time-domain, and frequency-domain were analyzed, highlighting the need to implement systems with a high sampling frequency. Additionally, extensive studies of different protection methods in HVDC transmission systems were conducted in [52,53].

To better integrate emerging technologies, hybrid power grids have also been considered a versatile and flexible solution. These architectures can harness the advantages of both grid types, albeit with more intricate control structures [54,55].

The need for isolation and the features of a determined RES interfacing system will ultimately depend on the specific needs of each project. According to the proposed objectives, different architectures and configurations must be chosen, as well as the topologies for power converters. For isolated DC–DC topologies, the design and sizing are of particular importance since there will be greater losses and electromagnetic interferences will directly

influence the operation of all devices. Thus, appropriate modulations and strategies aimed at increasing reliability, flexibility, and efficiency must be defined.

3. Isolated DC–DC Converter Properties, Topologies, and Modulations

The selection of topologies for interfacing RES-based generation technologies is always in consonance with the characteristics of the converter itself, namely, the power and voltage ratings, number of stages, added functionalities, and isolation requirements. As discussed in the previous section, the use of isolated topologies is reflected globally in a greater number of advantages, but to maximize efficiency, appropriate modulation techniques, as well as MPPT and utility grid connection algorithms, should also be chosen.

In medium- and high-voltage applications, renewable energy interface systems predominantly adopt a three-phase configuration, making the choice of topologies for each converter of utmost importance, with a particular emphasis on isolated DC–DC topologies. Nevertheless, considering the aforementioned advantages, isolation also plays a preponderant role in low-power single-phase systems. Given the high technological maturity of LFTs, they are widely used in numerous cases; however, in line with the technological assumptions for future smart grids, this conversion stage will necessarily have to present new and innovative functionalities.

These innovative features can only be achieved through the implementation of appropriate modulations and architectures in each power electronics system. In the case of isolated topologies, specifically DC–DC converters, the utilization of HFTs (or MFTs), supported by WBG semiconductors, is indispensable. By considering the transformer turn ratio ($N_t = N_1/N_2$), a broader range of voltage conversions is attainable, which endows these converters with increased flexibility, reliability, and compatibility with various devices. Additionally, these isolated stages offer advanced fault tolerance capabilities, effective mitigation of ground potential differences (e.g., ground loops), and enhanced immunity to noise and electromagnetic interference (EMI) [56]. Such attributes are particularly critical in circuits used for data transmission or analog signal applications.

Among the DC–DC isolated topologies, the dual active bridge (DAB) converter holds a prominent position and is widely utilized across a wider range of scenarios [57–59]. However, it is also important to note that various other topologies have been extensively studied in the literature. The selection of a particular topology depends on several factors, including the specific application scenario, control and implementation simplicity, power range conversion requirements, and the desired number of outputs.

3.1. Conventional Isolated Topologies

In the interface with RES-based generation technologies, among conventional isolated DC–DC converters, the flyback, forward, and push–pull topologies are commonly mentioned and utilized. These topologies are depicted in Figures 5–7, showcasing both their classic architecture and occasional variations. Despite having distinct characteristics, especially in terms of operating power, they are widely employed due to their simplicity, ease of control, and relatively high efficiency across a wide range of voltage levels. Consequently, the abovementioned isolated DC–DC topologies provide increased flexibility, are considered excellent cost-effective power electronics solutions, and given their technological maturity, are frequently found in a broad range of scenarios. Nonetheless, besides differences in operating power, these topologies also vary in transformer type, number of possible voltage outputs, and immunity to interference caused by semiconductor switching. Once again, both component selection and converter design play crucial roles in achieving the desired performance and efficiency.

3.1.1. Flyback

Ordering flyback, forward, and push–pull converters based on desired output power, the flyback converter presents the lowest nominal value. However, by increasing the voltage levels supported by WBG semiconductors and the power density of converters, and by including high-voltage gate drivers in control circuits, topologies that were previously limited to low-power applications are now being employed in a wider range of power solutions. Nevertheless, the selection of a specific topology also considers other significant factors, including associated costs, volume and weight, electrical stress, output noise, and input voltage range, among others.

Since the flyback converter generates a non-inverting output, its application in several devices is facilitated, eliminating the need for additional complementary circuits. Thus, this isolated DC–DC topology is regularly employed in low-power scenarios, such as power supplies and microinverter configurations for solar PV systems [60]. As shown in Figure 5a, it incorporates a single active switch (S_1), resulting in reduced costs, as well as switching losses. A coupled-inductor transformer is added to store energy during the on-time of S_1 and transfer it to the secondary side during the off-time [61]. It is important to note that current rectification is solely performed by the diode D_1, leading to an increased ripple in the output voltage waveform (V_{out}) and, consequently, lower efficiency. Moreover, the use of HFTs or MFTs may also be considered, thus providing not only galvanic isolation but also increasing the step-up ratio. Therefore, based on N_t and the duty cycle (D) applied to S_1, V_{out} is determined as follows [23]:

$$V_{out} = \frac{N_2\, D}{N_1\, (1 - D)} V_{dc} \tag{1}$$

With the use of a flyback converter, it is also feasible to obtain multiple DC outputs by adding extra windings to the HFT and employing suitable circuits and modulation techniques to regulate each individual output [62]. Depending on N_t and the implemented control circuit, these DC outputs can operate independently, which means the possibility of obtaining distinct voltage levels and connecting devices with differently rated power. However, as the number of DC outputs increases, the control complexity also escalates.

Regarding topology classification, the flyback converter is categorized as a single-ended configuration. In other words, only the primary winding of the transformer is connected to the power switches, whereas in double-ended topologies, the power switches are connected to both sides of the transformer. As a result, single-ended topologies do not support bidirectional power flow. In a flyback converter, the active semiconductor S_1 is connected to the primary winding, while the rectifying element, D_1, is linked to the secondary. Analyzing the transformer's B–H curve, the flux only exists in one quadrant, specifically from zero to positive values, without reversing direction. This leads to enhanced power handling capabilities and efficient conversion since the absence of bidirectional power flow reduces losses associated with reverse current and voltage stress.

However, when the flyback converter operates in discontinuous conduction mode (DCM), the primary side current stress of the HFT increases, leading to higher conduction losses and elevated peak currents. Additionally, the operation in DCM contributes to greater THD due to abrupt switching transitions and increased current ripple. This effect is aggravated as voltage ripple on the DC bus augments, which negatively impacts the converter's performance by increasing switching losses and reducing overall efficiency [63]. In DCM operation, switching and conduction losses tend to decrease at lower power levels given the reduced duty cycle and shorter conduction intervals. However, as the power increases, the current stress on the switching devices grows, leading to the need for thermal dissipation requirements. Additionally, core losses in the HFT remain significant

or even increase due to the higher flux density and frequency components associated with DCM operation. To mitigate these drawbacks, as shown in Figure 5b, interleaved topologies operating in continuous conduction mode (CCM) are often employed [64,65]. These topologies are more robust and efficient and exhibit lower voltage stress, as well as increased immunity to EMI. At higher power levels, current ripple, peak stress, and core saturation effects are significantly reduced. In the case of the conventional flyback converter, CCM operation is unpopular. Nonetheless, its performance can be improved by employing zero-voltage switching (ZVS) [66] or soft-switching techniques, which, in turn, require the inclusion of clamping circuits to the basic topology.

In the case of the interleaved flyback topology, the inclusion of two large magnetizing inductances (L_{m1} and L_{m2}) ensures that load variations do not impact the converter's performance [67]. However, it is worth noting that, apart from DCM and CCM, the converter can also operate in boundary conduction mode (BCM). This mode enables higher power density and improved output voltage power quality. Nevertheless, it comes at the cost of increased switching and gate drive losses compared to DCM and CCM.

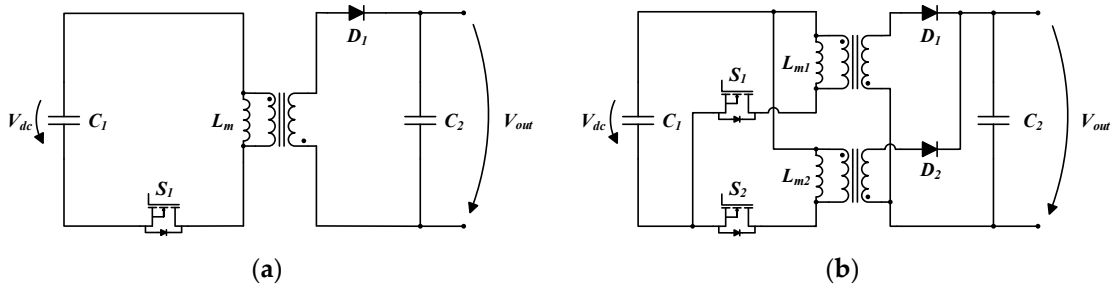

Figure 5. Isolated DC–DC flyback converter: (**a**) conventional; (**b**) interleaved flyback.

3.1.2. Forward

In industrial applications and motor drives, isolated DC–DC forward converters are commonly chosen due to their excellent voltage regulation and high efficiency. As illustrated in Figure 6a, similar to the flyback converter, the forward converter is classified as a single-ended topology, and a single active switch, S_1, is considered. Consequently, by adjusting D, a given input voltage, V_{dc}, may either be stepped up or stepped down. This versatility makes it suitable for various applications; however, it is important to note that this topology suffers from a poor transformer utilization ratio.

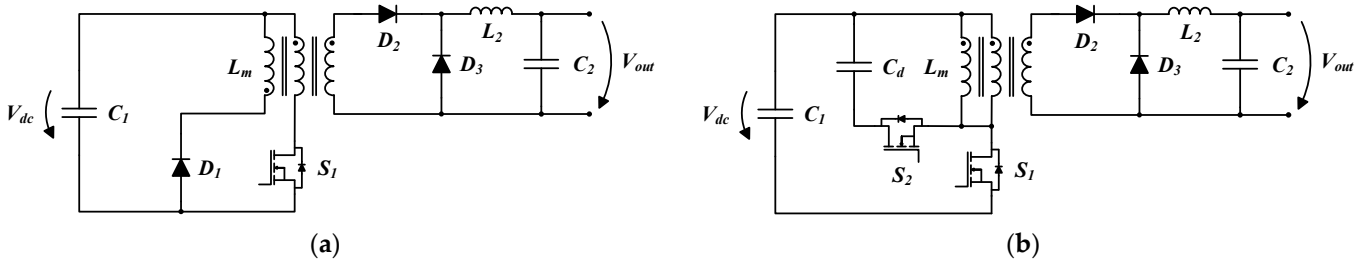

Figure 6. Isolated DC–DC forward converter: (**a**) conventional; (**b**) active clamp forward.

The improved efficiency exhibited by this topology is attributed to lower conduction losses and its ability to operate, commonly, both in DCM and CCM. Additionally, compared to flyback, the forward converter presents lower semiconductor voltage stress, as it only needs to handle the value of V_{dc} [68]. In contrast, the semiconductor S_1 of the flyback converter needs to withstand both V_{dc} and the reflected voltage of V_{out}.

Nonetheless, by recycling the energy stored in the transformer's leakage inductance, a forward topology with active clamp circuitry, as depicted in Figure 6b, significantly

enhances the overall efficiency of the power system [69]. This modification in the primary circuit enables further reductions in voltage stress and switching losses, as soft-switching is ensured. Despite operating in two quadrants, it is worth noting that an active clamp forward converter may experience high peak flux levels during startup and transient states. Additionally, since control complexity increases, this variant of the conventional forward converter is commonly used in devices and technologies that demand higher efficiency, reduced stress, and substantial power levels, such as the telecommunications sector and RES-based power elements.

3.1.3. Push–Pull

Unlike flyback and forward converters, a push–pull topology is classified as double-ended, offering several advantages in terms of transformer core utilization. As mentioned above, double-ended topologies are particularly well suited for high-power applications. Furthermore, the architecture of the push–pull converter allows for an extended D range, approaching values close to 100%. As demonstrated in Figure 7, the secondary stage of the converter includes two diodes, D_1 and D_2, connected to the secondary windings of the transformer [70,71]. Once again, these components are responsible for rectifying the current, which conveys a unidirectional nature to the power converter. However, in modern devices, these diodes are often replaced by active switches such as Si IGBTs, SiC MOSFETs, or GaN-based technology [72].

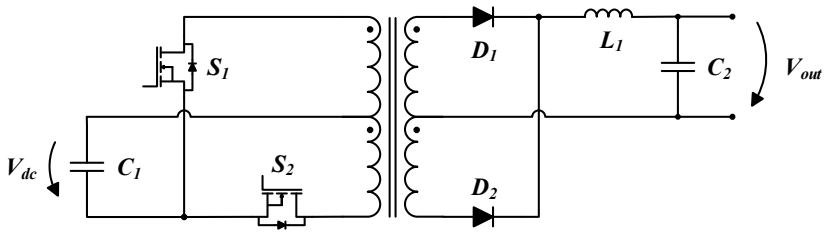

Figure 7. Conventional push–pull converter topology.

Therefore, similar to the forward converter, the push–pull topology is commonly employed in high-power scenarios that require an enhanced efficiency of conversion. Due to its symmetrical structure, the operation of the push–pull converter is balanced, which minimizes common-mode noise, EMI, and output current ripple. However, some drawbacks must be considered. The topology exhibits moderate complexity, and there is increased voltage stress on switches S_1 and S_2 during their off-state periods, approximately twice the value of V_{dc}. Additionally, the use of a center-tapped HFT adds to the cost and volume of the power converter, which can be a limitation in applications where it is vital to reduce the physical footprint, such as in RES-based generation systems [73].

3.1.4. Other Topologies

Based on conventional buck and boost structures, isolated versions have been analyzed in the literature, though less frequently. Their relevance is particularly evident in integrating RES-based systems in future microgrids and smart grids. As with non-isolated counterparts, their main function is to step-down or step-up a given V_{dc}, respectively. Isolated DC–DC converters rely on the principle of pulse width modulation (PWM), but in this case, V_{out}, is also determined by N_t. In terms of efficiency, isolated topologies significantly improve power dissipation and losses related to the leakage inductance (L_k), enhancing overall converter performance. However, the inclusion of galvanic isolation increases EMI levels, negatively impacting safety and the ability to effectively stabilize and regulate V_{out}.

On the one hand, isolated buck converters are commonly used in the telecommunications industry, automotive sector, and power supply devices. On the other hand, isolated

boost converters are primarily employed in high-voltage DC bus regulation and ESSs. However, both of them are highly suitable for the renewable energy sector, especially in microgrid applications, where voltage step-up or step-down functionalities are essential for efficient power management. Additionally, they can be utilized as an intermediate DC–DC stage between the solar PV modules and the corresponding grid-tied inverter. Based on the literature analysis, these topologies may be interconnected and associated with full-bridge converters, both in the inversion stage and in the rectification stage. Furthermore, isolated versions of zeta, SEPIC, and cuk converters are also available, as illustrated in Figure 8, showcasing multi-output structures [74]. These configurations are mentioned in [75], where an in-depth study on multi-output DC–DC converters is provided.

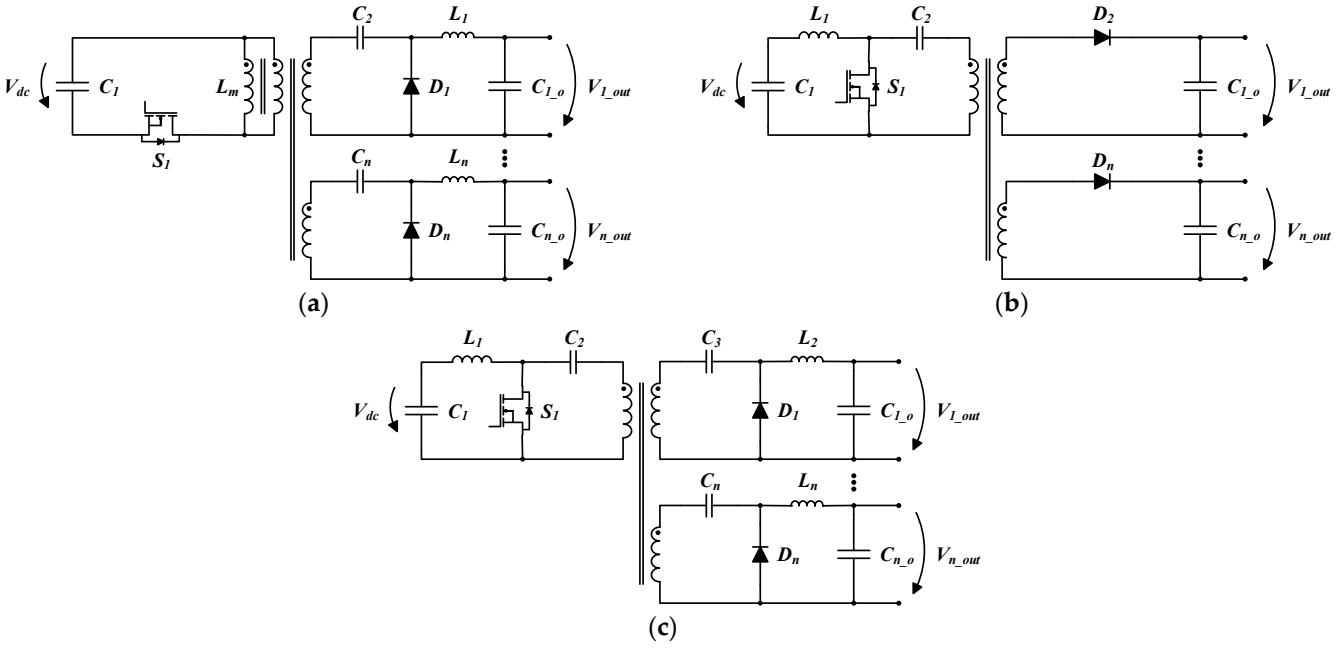

Figure 8. Conventional isolated multi-output DC–DC topologies: (**a**) zeta; (**b**) SEPIC; and (**c**) cuk.

The article not only discusses the fundamental topologies but also explores potential combinations between different structures and analyzes their applicability in various scenarios. However, these variations not only provide improved voltage regulation through N_t but also effectively mitigate the input and output current ripple. This capability is particularly important in RES-based generation elements where it is necessary to interface between power systems with different ground references, attenuate noise, and minimize the effects of switching transients. Additionally, these isolated converters facilitate stable V_{out} regulation even in the presence of load variations and fluctuations in V_{dc}.

3.2. Bridge-Based Isolated Topologies

Bridge-based isolated topologies, compared to the above-presented conventional structures, offer a broader range of advantageous features, making them the most commonly used converters in modern power electronics systems [76]. Similarly to the pushpull converter, bridge topologies are classified as double-ended, which allows for increased power handling capability. Among these properties, improved stability and voltage regulation are highlighted, as different modulation techniques can be easily implemented.

Depending on the specific topology, the voltage stress on semiconductor devices can be minimized, while simultaneously providing greater flexibility in voltage conversion. In other words, depending on the application scenario, these topologies enable both stepping down or stepping up a given V_{dc}. Moreover, excellent scalability and modularity are offered, i.e., there is great flexibility in interconnecting multiple isolated DC–DC bridge

converters in cascaded or parallel arrangements [77]. Multilevel configurations are particularly adequate for high-power scenarios where a given voltage or current needs to be divided among several isolated modules. Moreover, this modular characteristic enables increased redundancy and efficient fault mitigation within individual modules [78].

Furthermore, bridge-based topologies may also be easily adapted to enable bidirectional power flow. While this feature may not be essential in RES-based generation solutions, it plays a significant role in enhancing flexibility and versatility in the context of smart grids (e.g., for interfacing ESSs), while also reducing losses. Additionally, by incorporating active switches instead of passive components (e.g., diodes), recent and innovative modulation techniques and control algorithms may be more easily implemented, thereby improving the overall performance of the interface system [79].

3.2.1. Conventional Half-Bridge, Single Active Half Bridge, and Dual Half-Bridge

In isolated half-bridge topologies, as illustrated in Figure 9a, the inversion of a given V_{dc} is accomplished using two active semiconductor devices, S_1 and S_2, and a split DC bus constituted by capacitors C_1 and C_2. The windings of a transformer, ideally an HFT or an MFT, are connected to the midpoint of each arm, allowing the subsequent rectification of the signal on the secondary side of the converter.

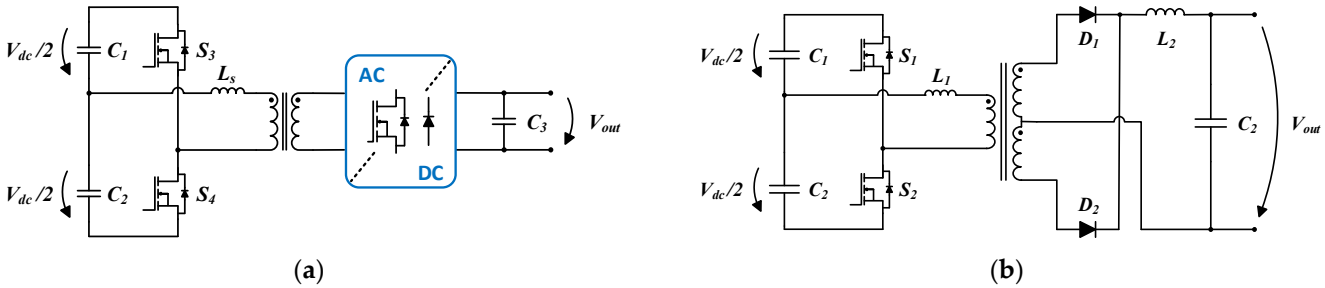

Figure 9. Conventional half-bridge isolated DC–DC converters' (**a**) structure and (**b**) topology.

In comparison with the conventional isolated DC–DC converters, particularly the push–pull topology (both double-ended), half-bridge configurations offer lower voltage stress as the value of V_{dc} is not exceeded in the semiconductor devices. Therefore, it is vital to carefully select the appropriate switching elements that best suit the requirements of the power electronics system. In addition, as previously described, there is no need to use transformers with multiple windings, leading to improved utilization of the transformer's core window and overall performance. Nevertheless, compared to other bridge topologies, the half-bridge converter provides simplicity and cost advantages due to its lower number of active switches. However, it is limited to voltage mode operation since maintaining voltage balance at the midpoint of the DC bus at ½ V_{dc} is crucial [80].

Therefore, in conjunction with a half-bridge topology based on active switches, the rectification block is equally important to ensure efficient energy conversion. As shown in Figure 9b, the conventional isolated asymmetrical DC–DC half-bridge employs a center-tapped HFT, typically resulting in a single DC voltage output. To obtain a higher number of levels and isolated outputs, extra circuits are required, which increases complexity and introduces noise. Thus, it is evident that the conventional half-bridge is not easily scalable, necessitating the use of additional HFTs to increase power levels. Regarding fault tolerance, ensuring continuous operation of the converter becomes extremely challenging if one of the semiconductors gets damaged, which indicates a lower level of redundancy. On the positive side, among the topologies depicted in Figures 9 and 10, the conventional half-bridge exhibits the lowest associated costs and complexity. This is because, for unidirectional arrangements, it is only necessary to control the half-bridge inverter.

In a single half-bridge converter, as the name suggests, only one switching stage is adopted, i.e., one side of the isolated DC–DC power converter operates in a passive mode for rectification purposes, while the other, specifically the inverting primary side, incorporates active semiconductor devices [81]. As illustrated in Figure 10a, signal rectification is achieved by connecting the secondary winding of the HFT to an arm constituted by two diodes (D_1 and D_2) and to the midpoint of the output split DC bus. On the other hand, a dual half-bridge (DHB) configuration has a bidirectional nature. However, as already indicated, this requirement is not mandatory when interfacing with RES-based generation technologies, despite the significant advantages it offers. As observed in Figure 10b, the primary and secondary sides of the transformer are symmetrical, i.e., rectification is now performed using a half-bridge topology with active switches [82]. In total, four switching devices are used, with a split DC bus on both sides.

Once again, due to the characteristics of bridge-based topologies, a half-bridge rectification stage offers greater redundancy, enhanced fault tolerance, and the generation of multiple independent DC outputs, thus demonstrating its flexibility and scalability. Additionally, thanks to the high modularity of the power converter, an interleaved DHB topology can easily be considered for a wide range of applications. In general, interleaved topologies may be described as a certain number of power converters connected in parallel to share a certain current among them. This type of topology offers significant advantages, such as low ripple frequency and losses, but they come with higher costs. Similarly to multilevel topologies, interleaved converters are commonly utilized in high-power scenarios to increase conversion efficiency and reliability.

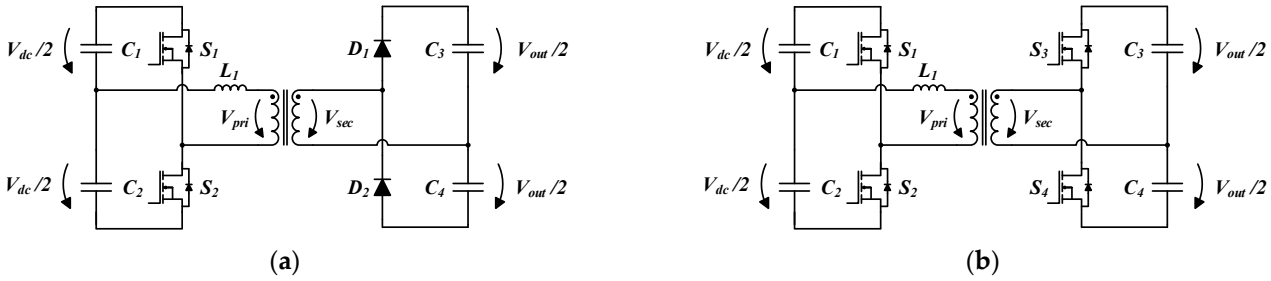

Figure 10. Half-bridge isolated DC–DC topologies: (**a**) single active half-bridge and (**b**) dual half-bridge.

3.2.2. Conventional Full-Bridge and Half-Full-Bridge

Despite the numerous advantages offered by isolated DC–DC half-bridge-based topologies, particularly in terms of cost and complexity reduction, the voltage conversion process is not entirely efficient. The semiconductors in the single switching arm operate in a complementary manner, resulting in a voltage across the primary winding that is half the value of V_{dc}. In contrast, in a full-bridge structure, as represented in Figure 11a, when a diagonal pair of active semiconductors is in the one-state, the voltage across the primary winding assumes the value of V_{dc} without the need to split the DC bus. As a result, for a given power level, the current flowing through the primary side of the HFT is half compared to a half-bridge topology, thus leading to higher efficiency.

In isolated DC–DC full-bridge converters, the rectifying stage, among different possibilities, may employ different topologies such as the conventional structure (as shown in Figure 11b), a half-bridge structure, a diode full-bridge, or even a full-bridge converter using active semiconductor devices. Similarly to the conventional isolated DC–DC half-bridge converter, the incorporation of a center-tapped HFT is also required, which constitutes one of the limitations compared to alternative rectifier stage topologies.

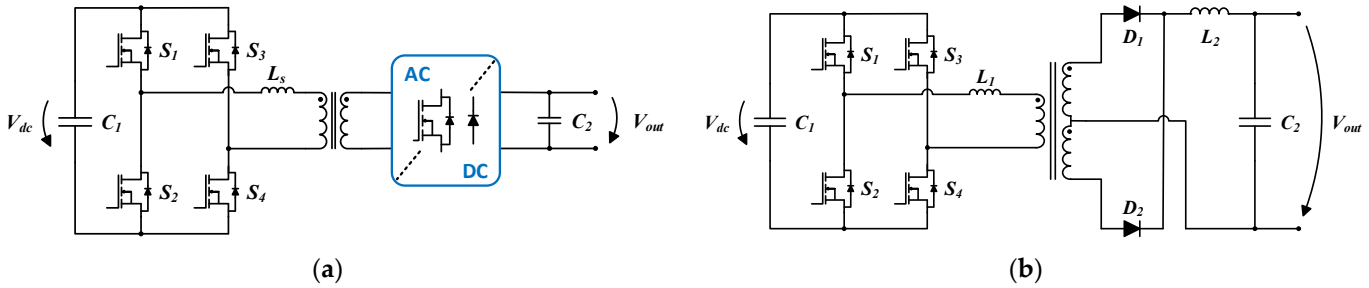

Figure 11. Conventional full-bridge isolated DC–DC converter (**a**) structure and (**b**) topology.

Therefore, an isolated DC–DC full-bridge topology, despite its moderate complexity, significantly improves the efficiency of conversion. Unlike half-bridge topologies, where each active semiconductor handles half the value of V_{dc}, in a full-bridge structure, each switching device must support V_{dc} entirely, which, consequently, reduces the current stress. Simplistically, by distributing the current among a larger number of semiconductors, both conduction and switching losses are minimized, particularly in high-power scenarios. In terms of costs, although the number of active semiconductors is doubled (four instead of two in the inverting stage), the number of capacitors is halved.

Since full-bridge structures are highly suitable for a wider input voltage range, they offer superior versatility in various application scenarios. Examples include their use in grid-tied inverters, motor drives, uninterrupted power supplies (UPSs), and, as expected, in the renewable energy sector. Globally, compared to isolated DC–DC half-bridge topologies, a full-bridge-based structure provides enhanced voltage regulation, increased redundancy, minimized switching stress, and the ability to operate at higher power levels. However, even in the case of isolated DC–DC half-bridge topologies, the rectification stage can be implemented using full-bridge-based structures, utilizing either diodes or active semiconductors such as MOSFETs or IGBTs. These mixed configurations, commonly referred to as half-full-bridge configurations, are shown in Figures 12 and 13 [83].

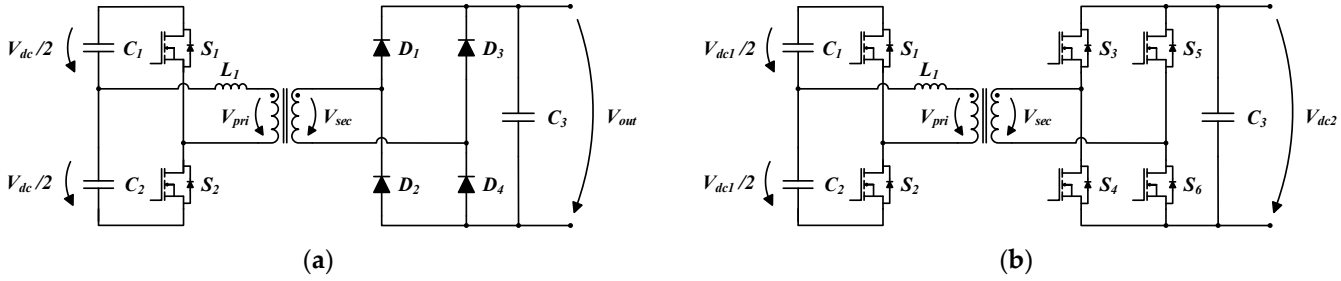

Figure 12. Half-full-bridge isolated DC–DC converters with (**a**) unidirectional power flow and (**b**) bidirectional power flow.

As previously mentioned, the converters used in the bidirectional topology shown in Figure 12b could be easily reversed [84]. In other words, the inversion of V_{dc} would be achieved using a full-bridge topology, which yields higher conversion efficiency, while rectification would be accomplished using a half-bridge structure [85]. However, as indicated in the section discussing half-bridge-based topologies, interleaved structures can also be implemented in these mixed configurations, as shown in Figure 13 [86]. The inverter stage is composed of an interleaved full-bridge topology, whereas rectification is accomplished using a half-bridge diode-based converter.

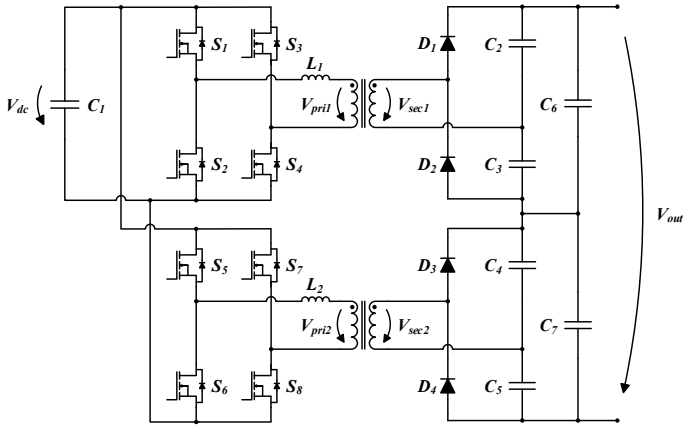

Figure 13. Unidirectional interleaved full–half-bridge isolated DC–DC converter.

3.2.3. Single Active Bridge and Dual Active Bridge

The single active bridge (SAB) and DAB converters utilize full-bridge structures in both the inverting and rectifying stages, as depicted in Figure 14. An active full-bridge converter is connected to the primary side of the HFT. However, the main difference lies in the topology and behavior of the rectifying stage. In the SAB converter, a full-bridge diode-based AC–DC converter is connected to the secondary winding of the HFT, which confers a passive behavior [87]. Subsequently, as is common practice in all DC–DC converters, a DC bus is included to smooth and stabilize a specific V_{out}. As a result, the power flow in this converter is unidirectional, requiring modulation on the DC-AC converter connected to the primary side of the HFT, while the secondary remains passive.

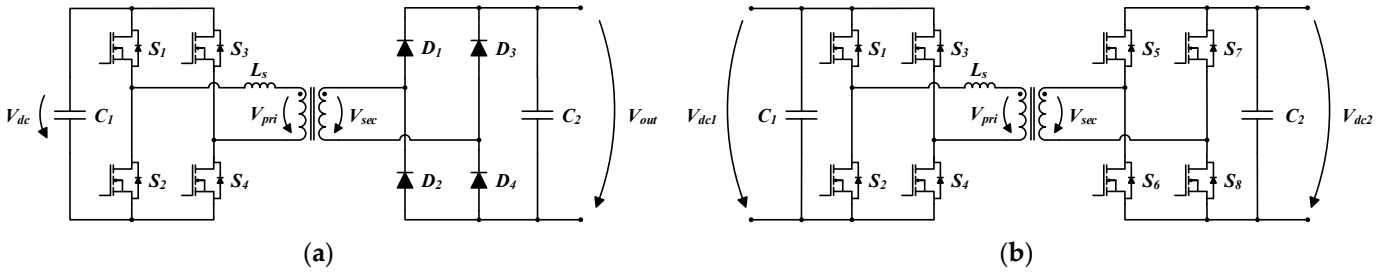

Figure 14. Full-bridge isolated DC–DC converters: (**a**) single active bridge and (**b**) dual active bridge.

The interface with power generation units involves the use of unidirectional structures. However, there are numerous advantages if the rectifying stage also operates actively and dynamically. Therefore, a DAB converter can be described as a symmetrical isolated DC–DC structure in which two full-bridge topologies, composed of active semiconductors devices, are connected to each winding of an HFT [88–91]. When interfacing with RES-based systems, bidirectional power flow is not the primary factor driving the adoption of a DAB converter. Instead, the focus is on the benefits of flexibility, scalability, and efficiency. In general, the independent control of each bridge aids in stabilizing the voltage on the primary or secondary side of the DAB converter, i.e., V_{dc1} and V_{dc2}, respectively. This feature plays a critical role in the operation of modern electronic solutions.

Additionally, it is possible to achieve soft-switching throughout the entire power range, which is not feasible, e.g., in half-bridge isolated topologies. With effective controllability over power flow, DAB converters exhibit naturally higher power density. This characteristic is extremely important in power electronics systems for interfacing with RESs, as it is desirable to implement compact and lightweight technologies [92].

Similarly to all bridge-based structures, DAB converters offer superior modularity, scalability, flexibility, and redundancy. To enable the interface with high-power systems, it

is particularly important to interconnect different bridge converters in cascade or parallel configurations, which form the common structures: (i) input-parallel/output-parallel (IPOP); (ii) input-series/output-series (ISOS); (iii) input-series/output-parallel (ISOP); and (iv) input-parallel/output-series (IPOS) [93,94]. By distributing the current and/or voltage through a larger number of active semiconductors, the stress on each device is significantly reduced, leading to improved overall performance and reliability.

In this respect, Figure 15 depicts the respective block diagrams that represent the abovementioned arrangements. However, the specific topology of each block should be selected based on the requirements of the power electronics solution [95]. If a full-bridge topology is chosen, these diagrams would indicate the connection of multiple DAB converters with different arrangements. Notwithstanding, half-bridge-based topologies could also be chosen for this purpose. As depicted in red in this figure, the complexity of control and modulation increases as the number of interconnected isolated DC–DC converters rises. However, as mentioned above, this results in lower semiconductor stress.

However, as a distinguishing feature, DAB also allows for the mitigation of harmonic content in V_{out}. By facilitating the implementation of loss-minimization techniques, such as ZVS, and appropriate modulation techniques, including phase-shift variations, EMI is significantly reduced. Moreover, the adoption of a DAB converter ensures, inclusively, compliance with grid interconnection standards, making them highly adequate for a broader range of operating scenarios. These key factors contribute to the widespread adoption of DAB converters in the most diverse power electronics systems.

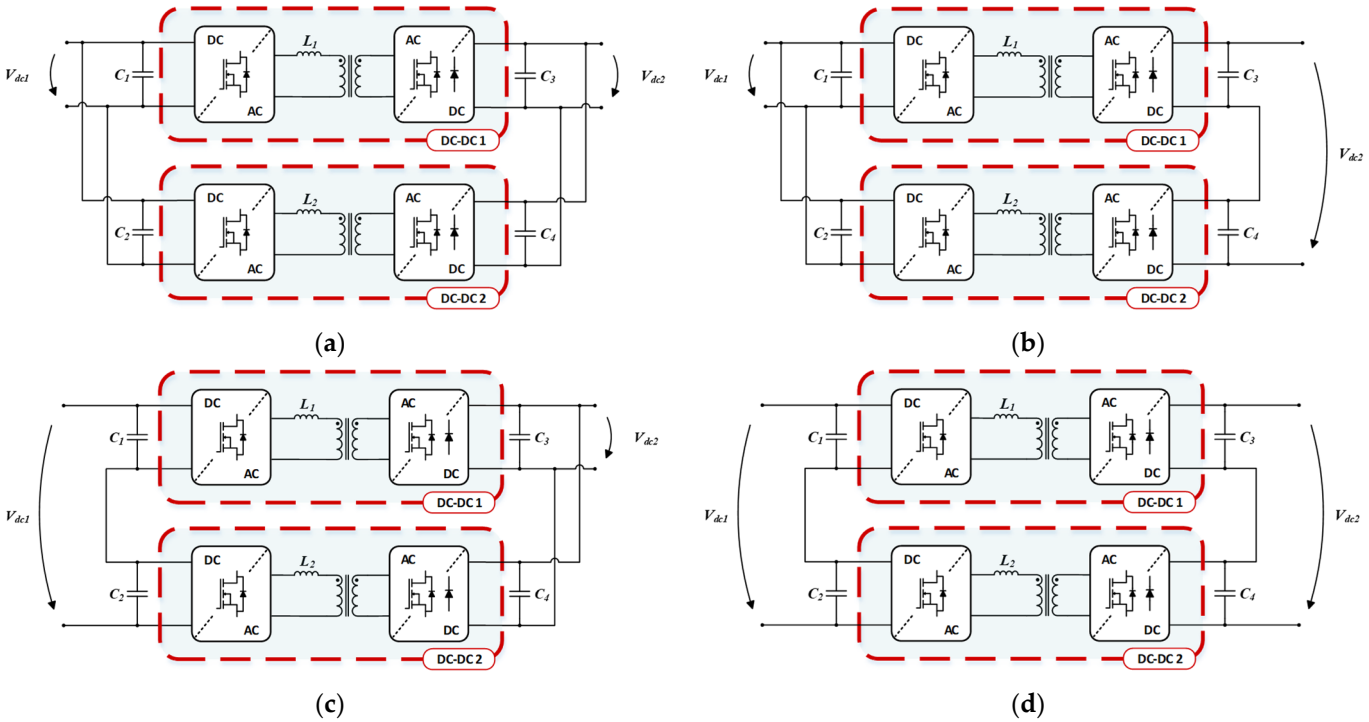

Figure 15. Arrangements for modular converters: (**a**) IPOP; (**b**) IPOS; (**c**) ISOP; and (**d**) ISOS.

The different arrangements depicted in Figure 15 are a consequence of the high modularity and scalability of bridge-based topologies, including DAB converters. However, multiport configurations can also be easily achieved by modifying the structure of the MFT [96]. As shown in Figure 16, the number of windings in the MFT corresponds to the number of independent input/output terminals [97]. Depending on the topology of each bridge and the power device connected to each terminal, the power flow can be either unidirectional or bidirectional. Each input/output terminal is galvanically isolated from

the others, while efficient and flexible energy exchange is enabled between them. Since the power electronics system is totally integrated, higher power density is obtained, simplifying the implementation of control algorithms and modulation techniques. Thus, Figure 16a presents the block diagram of an isolated bidirectional multiport DC–DC converter with four input/output terminals, while Figure 16b illustrates the same converter based on a quad active bridge (QAB) configuration [98–100].

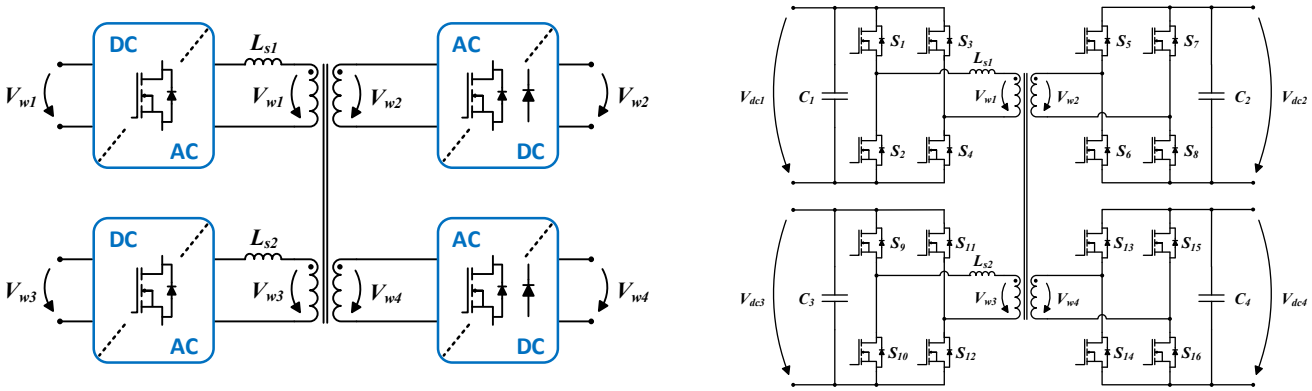

(**a**) (**b**)

Figure 16. Bidirectional isolated multiport DC–DC converter with four input/output terminals, represented by a (**a**) block diagram and (**b**) quad active bridge (QAB) topology.

Given that DAB converters are used to enable dynamic behavior in power interface systems during transient states, the role of modulation and control algorithms becomes crucial in optimizing the functionalities provided by the topology itself. Among other aspects, one of the key objectives is to mitigate current offsets by attenuating the effects of the magnetizing current of the HFT and the current that flows through L_k (i_{Lk}). In general, to improve voltage conversion and minimize losses, it is essential to incorporate the latest WBG devices, implement techniques aimed at improving power quality, and eliminate circulating currents. Additionally, it is equally important to address issues related to semiconductor stress, transformer saturation, and current spikes, which require a fast dynamic response from the power system.

In addition to adopting various strategies aimed at mitigating the aforementioned issues, the implementation of phase-shift modulation is widely accepted as a common practice. The consensus surrounding the adoption of phase-shift modulation is mainly due to its relative simplicity and ability to achieve high conversion efficiency. However, it is worth noting that, depending on the specific application and the chosen phase-shift variation, considerable levels of reactive power and circulating currents may be generated. Therefore, it becomes critical to extend the ZVS range, especially in situations where the primary side voltage, $V_{dc}1$, deviates from the value imposed by N_t, i.e., N_t $V_{dc}2$, where $V_{dc}2$ represents the secondary side voltage of the DAB converter [101].

Among the possible variations in phase-shift modulation, single phase-shift (SPS), dual phase-shift (DPS), extended phase-shift (EPS), and triple phase-shift (TPS) are highlighted, as compared in [102,103]. The key distinction lies in the number of degrees of freedom, i.e., the value assigned to each phase-lag angle, both between the two full-bridge converters that compose the DAB (outer phase angle, D_0), and within each bridge arm (inner phase angles, D_1 and D_2). The selection of a specific modulation technique depends on the application scenario, but generally, more intricate techniques offer a greater range of advantages in terms of efficiency [104]. In essence, D_0 regulates the direction and magnitude of power transfer within the DAB converter, while D_1 and D_2 angles contribute to enhanced performance and improved power quality.

Nevertheless, for any variant, all eight-semiconductor devices are constantly switching with a fixed D of 50%. In this regard, the phenomenon that enables power transfer in this isolated DC–DC converter is the phase difference between the squared voltage waveforms across each winding of the HFT, i.e., V_{pri} and V_{sec}. When these waveforms are phase-shifted, a voltage is induced across L_k and, consequently, a current will flow through it (i_{Lk}). Depending on whether the phase difference is positive or negative, the direction of i_{Lk} will vary accordingly, as well as the power flow direction in the DAB converter. In other words, if V_{pri} leads V_{sec}, power will flow from the primary to the secondary side. Conversely, if V_{pri} lags behind V_{sec}, the opposite will occur. Therefore, adjusting this phase difference regulates power transfer, both in terms of direction and magnitude.

In power systems where V_{dc1} closely approximates V_{dc2}, SPS modulation is commonly utilized. Among the four aforementioned variations, it is the least complex, despite providing satisfactory practical results. However, a single degree of freedom is considered, D_0, which may result in increased reactive power generation [105]. The signals applied to semiconductors S_1 and S_3 are 180 degrees out of phase, as well as S_5 and S_7. The value of D_0 is applied to S_5, which indicates the phase difference between S_1 and S_5.

In turn, for DPS modulation, an extra degree of freedom, D_1, is introduced along with D_0. D_1 is applied to S_3, considerably improving DAB's efficiency, particularly in expanding the ZVS range. Moreover, this modification allows for the generation of a three-level waveform across V_{pri} and V_{sec}, which effectively contributes to reducing reactive power and total harmonic distortion (THD) produced by the converter [106].

In turn, EPS and TPS modulations are used in specific cases. Regarding the triggering gate signals applied to each switching device, the difference lies in the value applied to S_7. TPS modulation introduces an additional degree of freedom, D_2, which totals three phase-lag angles with respect to S_1. The control complexity substantially increases, but so does the conversion efficiency, as indicated in [107–109]. However, it should be noted that the number of applications that require the use of such modulation is more limited, whereas the use of the EPS technique is directed towards power solutions that require the transfer of higher power magnitudes within a shorter time period. Both techniques enhance the converter's flexibility, leading to greater precision and reduced losses [110,111].

Therefore, the summary of gate signal values applied to each switching device is presented in Table 1. Since all gate signals are phase-shifted from the value assigned to S_1, this signal is regarded as the reference (Ref.) to which the phase angles (degrees of freedom) will be added. Nonetheless, as expected, the signals applied to the bottom semiconductors of each arm are complementary to the ones depicted in the same table.

Table 1. Gate signals applied to the top arm semiconductors for SPS, DPS, EPS, and TPS modulation.

	S_1	S_3	S_5	S_7
SPS	Ref.	Ref. + 180°	Ref. + D_0	S_5 + 180°
DPS	Ref.	Ref. + D_1	Ref. + D_0	S_5 + D_1
EPS	Ref.	Ref. + D_1	Ref. + D_0	S_5 + 180°
TPS	Ref.	Ref. + D_1	Ref. + D_0	S_5 + D_2

3.2.4. Series Resonant Full-Bridge-Based Topologies

Achieving ZVS across a wide range of output voltage and power is a major challenge in DAB converters. To overcome this issue, phase-shift modulation techniques with multiple degrees of freedom have proven to be an excellent solution. However, alternative approaches involving circuitry modifications can also be effective.

Among these changes, the inclusion of a series resonant tank into the conventional DAB topology (FB-LC-DAB) has shown promising results, as exemplified in Figure 17a,

in which an LC resonant tank is connected to the windings of a single phase [112] and three-phase [113] HFTs. Additionally, the inclusion of an LC series resonant tank in a mixed full–half-bridge converter topology is studied in [85]. On the other hand, LLC resonant converters have demonstrated high efficiency in voltage conversion, providing increased power density, as shown in Figure 17b, where a diode bridge is integrated on the secondary side of the HFT for rectification [114]. Nonetheless, these LLC resonant tanks may even be included in multilevel topologies, as indicated in [115], or in hybrid configurations [116]. Furthermore, Figure 17c presents a bidirectional version, replacing the diode bridge with a full-bridge converter equipped with active switches and adding a resonant capacitor on the secondary side. This modified converter is referred to as a resonant CLLC converter [117,118]. Moreover, as mentioned in [119] and depicted in Figure 17d, the incorporation of a CLC resonant tank is considered. Figure 17e introduces a complementary approach by proposing an LCL variant [120,121].

In summary, isolated resonant DC–DC converters offer a broader range of advantages in terms of power density and ease of voltage conversion. Their operation under ZVS conditions minimizes switching losses, leading to improved thermal performance and increased reliability [122]. Additionally, as the name suggests, these converters operate at resonant frequencies, effectively attenuating HF noise. Thus, the need for additional filtering components is eliminated, significantly reducing EMI [123].

According to the aforementioned advantages, the utilization of resonant converters is particularly well suited for high-power applications [124]. A key feature of these topologies is their ability to enhance load regulation, as the control over the output voltage is more precise, stable, and adjustable in response to load changes. Furthermore, the attenuation of HF components reduces the voltage waveforms' THD, thereby improving the power quality. However, achieving optimal performance requires the adoption of suitable modulation techniques, components, and control algorithms, as well as careful design considerations for the resonant tank and other crucial components.

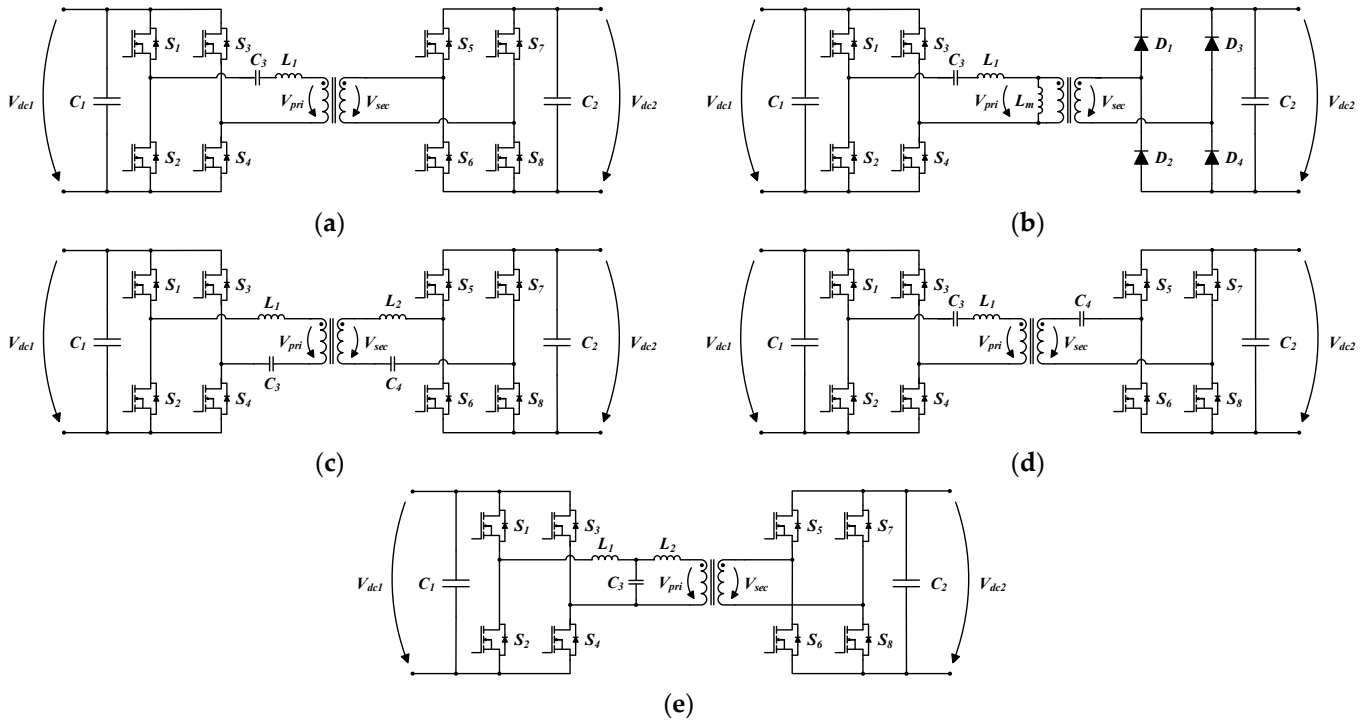

Figure 17. Series resonant isolated DC–DC converters: (**a**) bidirectional LC DAB; (**b**) unidirectional LLC; (**c**) bidirectional CLLC; (**d**) bidirectional CLC; and (**e**) bidirectional LCL.

As shown in Figure 18a and mentioned in [125,126], a center-tapped LC series resonant DAB (CT-LC-DAB) converter is proposed to eliminate backflow power by blocking reverse current. Moreover, in the same article, a comparative analysis is conducted with FB-LC-DAB and center-tapped L series resonant DAB (CT-L-DAB) converters, as illustrated in Figure 18b and mentioned in [127]. On one hand, the CT-L-DAB is unable to prevent backflow power, leading to higher conduction losses. On the other hand, the conventional FB-LC-DAB topology incurs significant switching losses due to hard switching. Therefore, the CT-LC-DAB topology emerges as a solution that addresses the limitations of the compared topologies in this article. As added functionality, it also enables operation in both DCM and BCM by implementing suitable modulation techniques.

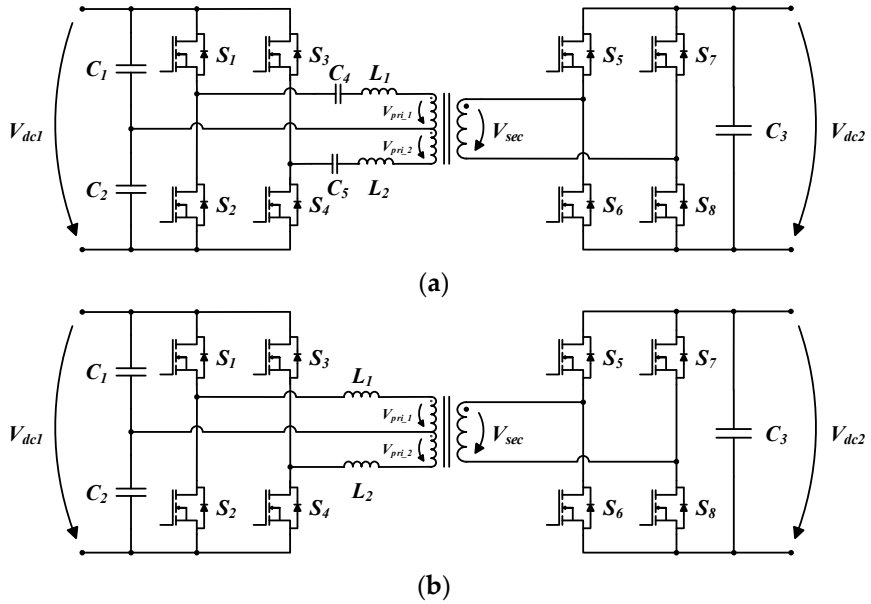

Figure 18. Series resonant isolated DC–DC converters: (**a**) CT-LC-DAB and (**b**) CT-L-DAB.

3.2.5. Other Full-Bridge-Based Topologies

In the literature, conventional isolated DC–DC topologies are sporadically combined with bridge-based structures to obtain enhanced flexibility and efficiency. Therefore, in [128], the utilization of an integrated full-bridge forward converter for battery charging and discharging is proposed. Unlike DAB and conventional forward converters, the proposed configuration incorporates an HFT with three windings, one of which has a center-tapped structure, as shown in Figure 19a. As mentioned in this paper and reinforced in [128], this bidirectional topology exhibits low-input and -output current ripple and high voltage ratio. Another example in the literature is the utilization of a full-bridge/push–pull converter, as shown in Figure 19b [129,130].

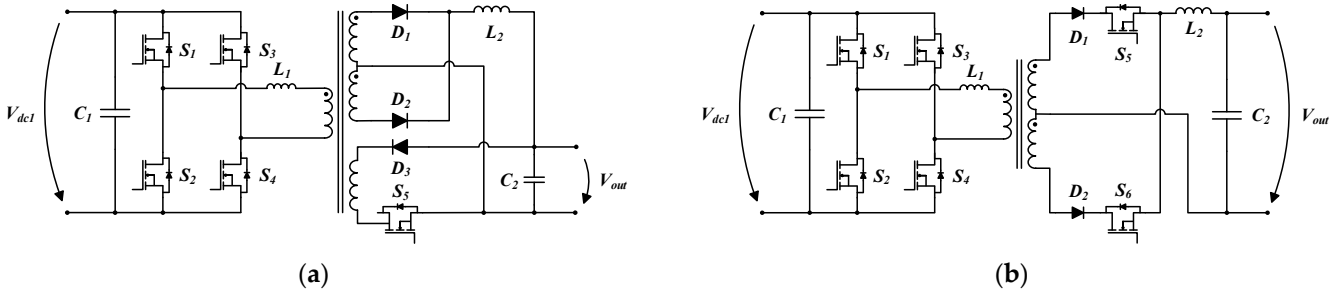

Figure 19. Hybrid topologies combining full-bridge structures with (**a**) forward and (**b**) push–pull topologies.

As shown in Figure 20, isolated current-fed topologies are also usually documented. Facing voltage-fed topologies, they exhibit shoot-through immunity and low-current stress, making them particularly suitable for low-voltage, high-current applications. In [131], the use of L-type full-bridge, full-bridge push–pull, and L-type half-bridge converters is mentioned. In these topologies, compared to voltage-fed converters, the input current ripple is reduced, as well as N_t. This characteristic is further enhanced in the converters depicted in Figure 20a,b as they employ interleaved variants.

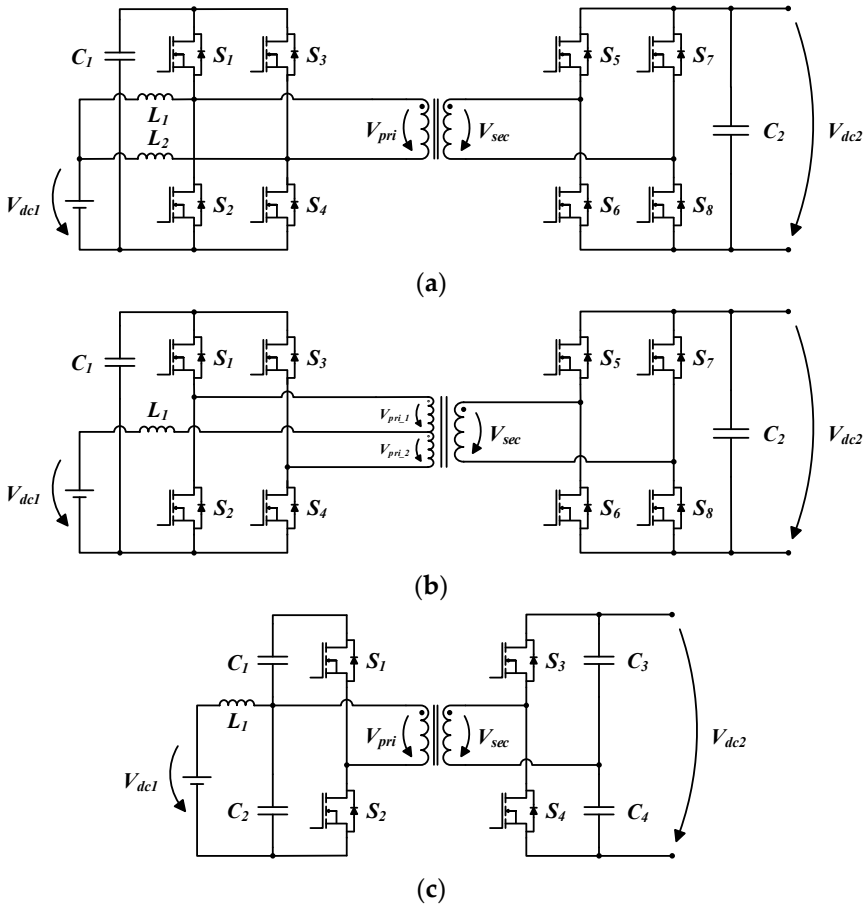

Figure 20. Current-fed isolated DC–DC converters: (**a**) L-type full-bridge; (**b**) full-bridge push–pull; and (**c**) L-type half-bridge.

3.3. Multilevel Topologies

The use of multilevel topologies, as extensively studied and widely adopted, is strongly recommendable in high-power scenarios. As the name suggests, in these types of converters, the voltage and/or current are distributed among multiple active semiconductors, which helps to minimize stress on each individual device. Consequently, the reliability of such power solutions is enhanced, while achieving improved conversion efficiency. Therefore, the application of multilevel topologies is highly recommended, not only in medium and high-power scenarios, but also in systems that prioritize power quality, such as grid-tied inverters, EV chargers, and RES interfacing systems.

In addition, multilevel converters are well suited for power electronics solutions demanding increased power density. The generation of multiple voltage levels assists in lowering stress on each active semiconductor and minimizes EMI [132]. This feature is particularly beneficial in EV chargers, as efficient voltage conversion is critical for battery charging and discharging operations. It is intended to extend the battery's lifecycle by avoiding potential overcharging and deep discharges and ensuring precise voltage regulation. As an additional feature, multilevel topologies are also well suited for the

implementation of EV fast-charging stations, which is becoming increasingly important and convenient to users due to the growing concern over range anxiety.

In summary, depending on the system requirements, multilevel topologies offer significant advantages over traditional topologies, including improved efficiency, power quality, reliability, and performance.

3.3.1. Multilevel DAB-Based NPC Converter

One of the most commonly used multilevel configurations is based on the incorporation of neutral point clamped (NPC) topologies. As indicated in [133], they are considered a variant of the DAB, commonly referred to as multilevel DAB (ML-DAB) converters. As illustrated in Figure 21, at least one of the full-bridge stages that compose the traditional DAB converter is replaced by an NPC converter, which generally allows for higher efficiency and the capability to operate higher power levels [134]. For all the documented cases, phase-shift modulation techniques are equally implemented; however, the major difference lies in the number of voltage levels that can be obtained in V_{pri} and V_{sec}.

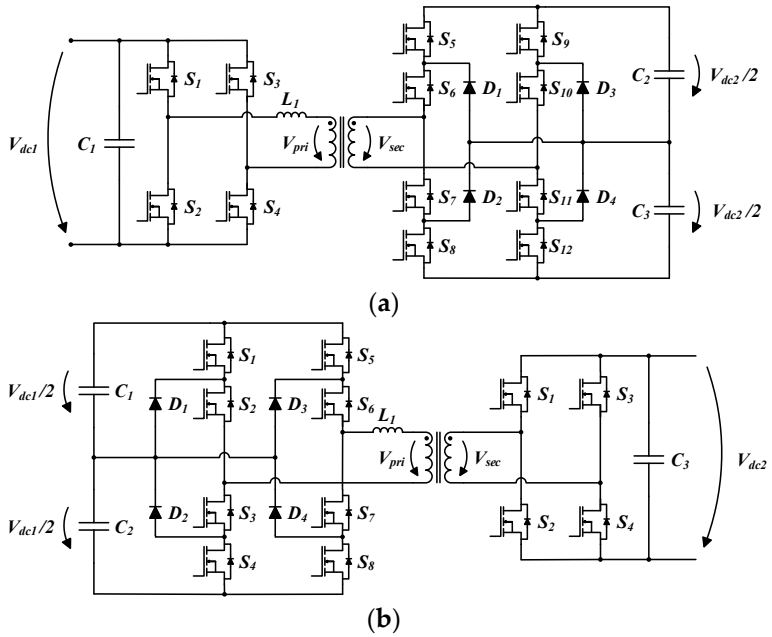

Figure 21. ML-DAB based on full-bridge and NPC converters with configuration: (**a**) boost and (**b**) buck.

Therefore, Figure 21a illustrates the operation of the ML-DAB converter based on a boost configuration, where the NPC topology is connected to the secondary side of the MFT. With this arrangement, V_{pri} commonly achieves two voltage levels, while V_{sec} can attain five levels [135]. Conversely, in a buck configuration, the opposite occurs, with five voltage levels obtained in V_{pri} as the NPC topology is connected to the primary windings [136]. As shown in Figure 21b, by utilizing a full-bridge converter, two voltage levels are once again obtained, this time regarding V_{sec}. However, depending on the adopted modulation and topology, it is also possible to obtain three voltage levels in the windings of the MFT.

Furthermore, as studied in [137,138], an NPC converter can potentially be connected on both sides of the MFT. As should be expected, the degrees of freedom increase, which reduces the simplicity of the modulation technique. Conversely, it enhances flexibility and further improves performance. In addition, active switches are not subject to high-voltage stress since they do not need to withstand the total DC bus voltage. As a result, costs are reduced, and the switching and conduction losses are minimized.

Nevertheless, the number of voltage levels may vary depending on the specific NPC topology. As suggested in [139], the ideal scenario is to obtain multiple voltage levels in V_{dc1} and V_{dc2}; however, this would significantly increase the number of degrees of freedom. Obtaining optimal values for each phase-lag angle and ensuring voltage balancing across the DC bus capacitors pose significant challenges. As a result, implementing a ML-DAB converter with multiple degrees of freedom is impractical, despite the significant energy efficiency benefits it would offer. To obtain three (or more) voltage levels, NPC converters based on half- and full-bridge structures are considered, as depicted in Figure 22.

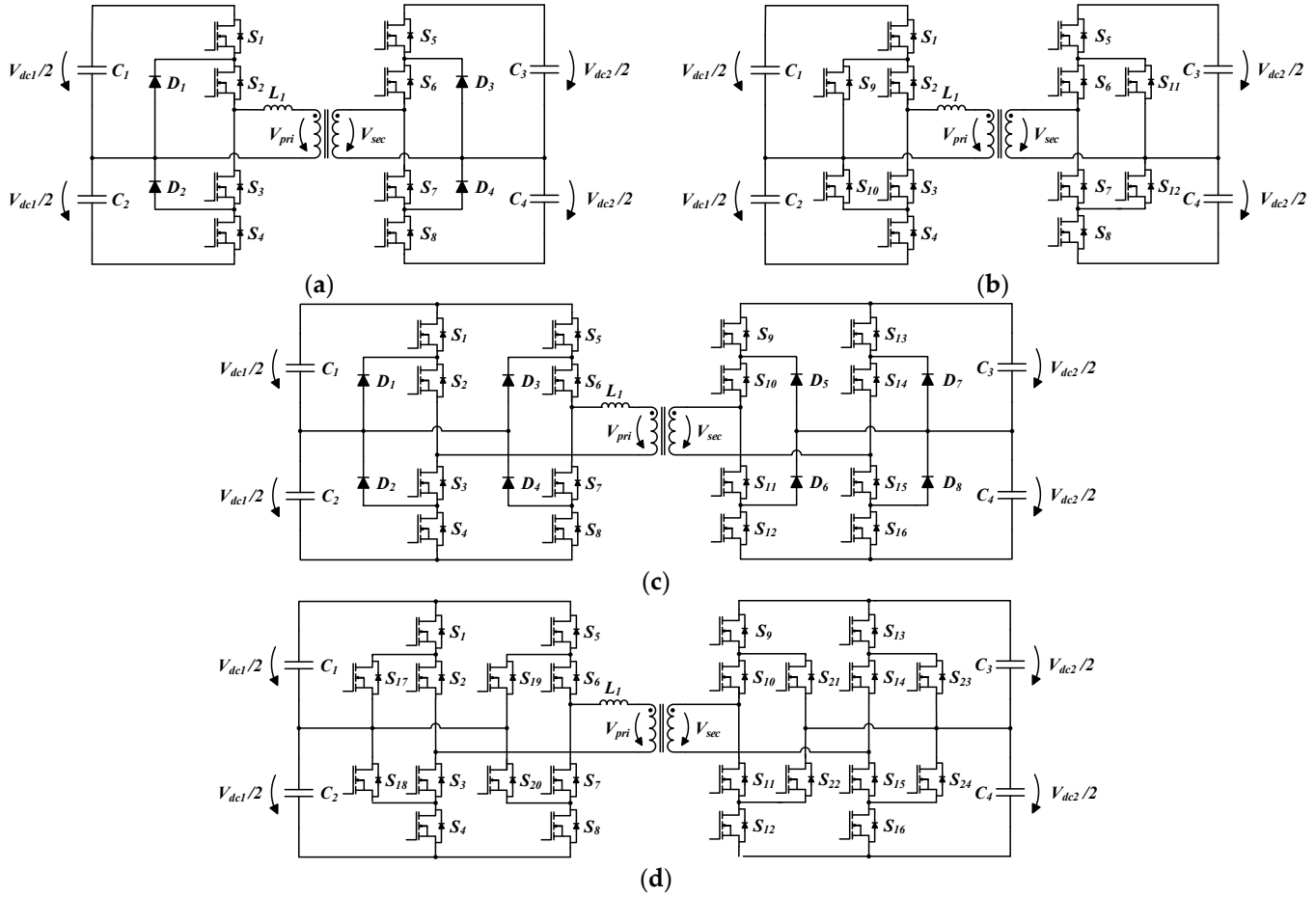

Figure 22. Three-level DAB based on NPC converters: (**a**) half-bridge DNPC-DAB; (**b**) half-bridge ANPC-DAB; (**c**) full-bridge DNPC-DAB; and (**d**) full-bridge ANPC-DAB.

Notwithstanding, the selection of each topology depends on the specific requirements of the power electronics system, leading to varying performance levels. Among the ML-DAB converters based on NPC converters, the diode NPC (DNPC-DAB) and active NPC (ANPC-DAB) topologies are highlighted. These topologies can be implemented in both half-bridge and full-bridge configurations, and, once again, the complexity of the modulation will vary accordingly [140,141].

The main features of DNPC-DAB and ANPC-DAB configurations were compared in [142], highlighting the greater suitability of ANPC-DAB topologies for achieving ZVS and soft-switching. As mentioned, they provided reliable voltage clamping for all switches but also redundant zero switching states. It was also indicated that adopting ANPC-DAB instead of DNPC-DAB results in better loss distribution and balanced power devices.

3.3.2. Modular Multilevel Converter (MMC)

Similarly to multilevel topologies, MMCs are specifically designed for high- and very-high-power solutions [143]. This configuration is considered a distinct type of multilevel converter, where multiple submodules are cascaded to divide a high value of V_{dc}. Although MMC topologies are commonly used in three-phase systems, Figure 23, for the sake of simplicity, depicts simplified single-phase architectures, both in half-bridge and full-bridge configurations [144]. However, what sets apart each MMC configuration is the chosen topology for the submodules [145]. Considering the aforementioned points, MMCs are recognized as a highly complex configuration that, conversely, provides substantial flexibility, modularity, and scalability. As a result, they allow for multiple arrangements among submodules and even across multiple MMCs, offering numerous possibilities regardless of the power solution. Their scalability allows effortless adaptation to different voltage and power levels by simply adding or removing specific submodules.

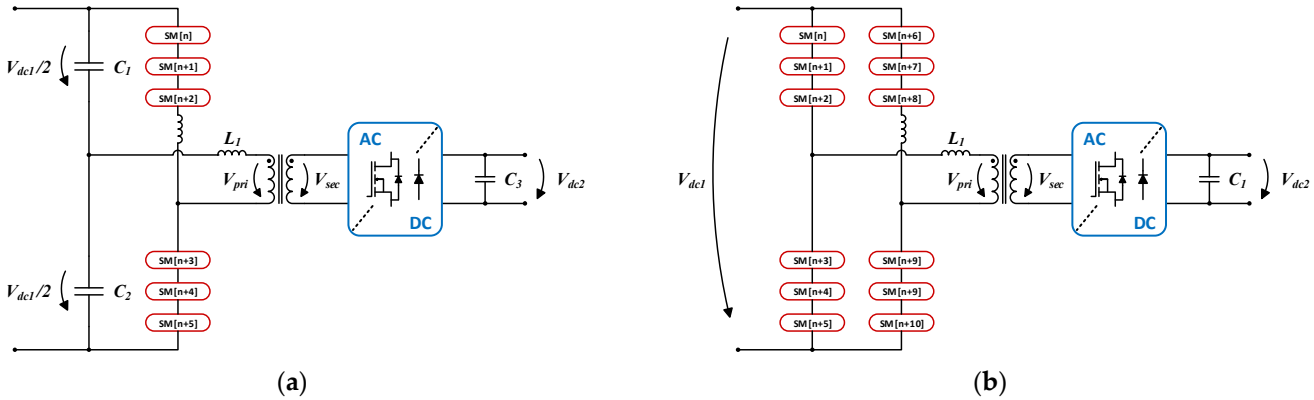

Figure 23. Conventional structure of a MMC converter, considering: (**a**) half-bridge configuration and (**b**) full-bridge configuration.

According to these characteristics, MMCs are frequently employed in power electronics solutions for energy transmission and distribution, particularly in HVDC transmission, flexible AC transmission systems (FACTSs) [146], and large-scale grid-connected renewable energy systems. Accounting for these application scenarios, MMC structures are highly suitable for high-voltage and high-power solutions due to their enhanced reconfigurability, redundancy, and fault tolerance. Furthermore, they play a crucial role in achieving efficient voltage conversion and mitigating power quality issues, including THD [147]. However, issues related to EMI are also considered [148].

The number of voltage levels produced and applied to the windings of the MFT is determined by the modulation technique and the chosen number of submodules. However, the main challenge encountered in MMCs lies in regulating the voltage across the DC bus of each submodule. Thus, extensive research has been conducted to explore different techniques for effectively stabilizing the submodule voltage, as documented in [149–153]. By precisely controlling this voltage value, the MMC achieves the desired output with increased performance.

To ensure system balance, each submodule is typically constructed with equal topologies. As common practice, depending on the power solution, these submodule topologies can vary from half-bridge structures to full-bridge-based topologies or even isolated stages like the DAB converter, as shown in Figure 24 [154–156]. As another example, each submodule can also be based on multiple stages with independent outputs, allowing for the distribution of different feeders. Despite operating as an isolated DC–DC structure, MMCs can also be interconnected with three-phase AC power distribution and transmission systems, fulfilling the role of voltage rectification.

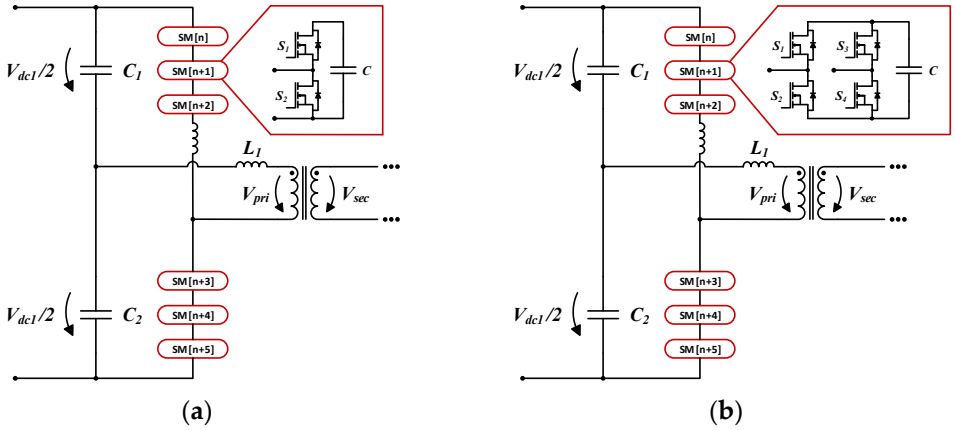

Figure 24. Examples of submodule topologies for MMCs: (**a**) half-bridge and (**b**) full-bridge.

4. Comparative Discussion of Isolated DC–DC Topologies

To reinforce the merits of the previously discussed isolated DC–DC topologies, this section presents a detailed comparative study. This analysis, summarized in Table 2, mainly focuses on the key trade-offs and electrical characteristics of each converter, considering efficiency, cost, complexity, flexibility, and resilience.

The above-mentioned factors are critical for integrating DC–DC converters into RES-based systems and smart grids, guiding the selection of the most appropriate topology for each application. This choice largely depends on the converter's operational power range, as well as the trade-offs between cost and complexity. Specific applications may require more efficient topologies, aiming to maximize power density, minimize switching losses, enhance waveforms, or meet given power grid integration requirements.

The control complexity of each isolated DC–DC converter is classified in Table 2 as low, medium, and high. Moreover, the table above highlights a potential bibliographic reference for each topology, indicating a relevant study or work where the respective converter has been analyzed or applied. It is also worth noting that the order in which the converters appear aligns with the sequence of illustrations presented throughout this review paper, ensuring consistency between the textual discussion and visual representations. The comparative analysis primarily concerns the physical characteristics of the converters, providing an overview of the number of switching devices (#S), diodes (#D), inductors (#L), capacitors (#C), and transformers (#T) used in each topology.

In this context, large-scale RES-based power systems, such as hydropower plants, wind farms, and utility-scale solar PV parks, demand efficient and scalable conversion solutions. Multilevel topologies, including MMC- and DAB-oriented NPC variants, have emerged as reliable and widely adopted solutions in the renewable energy sector. These topologies inherently offer high-quality waveform generation and enable seamless integration of RESs into power transmission and distribution grids.

In recent years, SSTs have gained prominence as a promising alternative for facilitating the integration of RESs into the power grid, providing advanced and additional interface functionalities. One of their key advantages is the ability to mitigate voltage and frequency fluctuations caused by the intermittent nature of RES generation. By implementing dynamic control mechanisms, SSTs effectively reduce the adverse effects of power variations in wind farms and solar parks, thereby enhancing power quality and improving overall grid stability. Thus, DAB converters and corresponding variants assume a central role in the development of SSTs, offering high efficiency, modularity, and flexibility. Their structure enhances the electrical interface between multiple DC buses, facilitating the direct integration of solar PV systems, ESSs, and DC-native loads into the power grid. Nevertheless, the implementation

of advanced control algorithms and phase-shift modulation techniques is the feature that optimizes power transfer in such topologies, improving the performance under various operating conditions. These characteristics appoint DAB converters as a robust and versatile solution, not only for RES applications but also for EV charging systems and hybrid AC/DC power grids.

Table 2. Comparison of isolated DC–DC converters, with references, differentiating between conventional low-power, bridge-based, and multilevel topologies. It presents key design parameters, including the number of switching devices (#S), diodes (#D), inductors (#L), capacitors (#C), and transformers (#T), along with a classification regarding control complexity.

Classification	Topology	Ref.	#S	#D	#L	#C	#T	Control Complexity
Conventional Low-Power Converters	Flyback	[61]	1	1	1	2	1	Low
	Interleaved Flyback with $n_t = T$	[65]	n_t	n_t	n_t	2	n_t	Low
	Forward	[68]	1	3	2	2	1	Low
	Active Clamp Forward	[69]	2	2	2	3	1	Low
	Push–Pull	[71]	2	2	1	2	1	Low
	Multi-Output Isolated Zeta	[75]	1	n_o	$1 + n_o$	$1 + 2n_o$	1	Medium
	Multi-Output Isolated SEPIC	[75]	1	n_o	1	$2 + n_o$	1	Medium
	Multi-Output Isolated Cuk	[75]	1	n_o	$1 + n_o$	$2 + 2n_o$	1	Medium
Bridge-Based Converters	Isolated Asymmetrical Half-Bridge	[80]	2	2	2	3	1	Low
	Single Active Half-Bridge	[81]	2	2	1	4	1	Low
	Dual Half Bridge (DHB)	[82]	4	0	1	4	1	Medium
	Bidirectional Half-Full Bridge	[84]	6	0	1	3	1	Medium
	Uni. Interleaved Full-Half Bridge with $n_t = T$	[86]	$4n_t$	$2n_t$	n_t	$1 + 3n_t$	n_t	Medium
	Single Active Bridge (SAB)	[87]	4	4	1	2	1	Low
	Dual Active Bridge (DAB)	[90]	8	0	1	2	1	High
	Quad Active Bridge (QAB)	[99]	16	0	4	4	1	High
	Series Resonant LC-DAB	[112]	8	0	1	3	1	High
	Series Resonant LLC-SAB	[114]	4	4	2	3	1	High
	Series Resonant CLLC-DAB	[117]	8	0	2	4	1	High
	Series Resonant CLC-DAB	[119]	8	0	1	4	1	High
	Series Resonant LCL-DAB	[121]	8	0	2	3	1	High
	Series Resonant CT-LC-DAB	[126]	8	0	2	5	1	High
	Series Resonant CT-L-DAB	[127]	8	0	2	3	1	High
	Hybrid Full Bridge-Forward	[128]	5	3	2	2	1	Medium
	Hybrid Full Bridge-Push-Pull	[129]	6	2	2	2	1	Medium
	Current-Fed L-type Full-Bridge	[131]	8	0	2	2	1	High
	Current-Fed Full-Bridge Push-Pull	[131]	8	0	1	2	1	High
	Current-Fed L-type Half-Bridge	[131]	4	0	1	4	1	High
Multilevel (ML) Converters	Boost ML-DAB	[135]	12	4	1	3	1	High
	Buck ML-DAB	[136]	12	4	1	3	1	High
	Three-Level Half-Bridge DNPC-DAB	[142]	8	4	1	4	1	High
	Three-Level Half-Bridge ANPC-DAB	[141]	12	0	1	4	1	High
	Three-Level Full-Bridge DNPC-DAB	[137]	16	8	1	4	1	High
	Three-Level Full-Bridge ANPC-DAB	[138]	24	0	1	4	1	High
	MMC-DHB with n_m Half-Bridge Submodule	[155]	$2n_m$	0	3	$4 + n_m$	1	High
	MMC-DHB with n_m Full-Bridge Submodule	[156]	$4n_m$	0	3	$4 + n_m$	1	High

The need for integrating emerging technologies has driven the adoption of multiport isolated DC–DC converters in distributed generation systems. Variants such as the DHB,

SAB, and DAB provide highly flexible solutions, enabling optimized control over the magnitude and direction of bidirectional power flow. Additionally, isolated multiport DC–DC converters, which may include the triple active bridge (TAB) and the QAB, are highlighted in the literature as widely employed in microgrid applications, particularly in the integration of hybrid solar PV-ESS.

For microinverters, often used in individual solar PV modules, the need for galvanic isolation is not always a fundamental requirement. However, due to safety concerns and regulatory compliance, conventional low-power topologies, such as flyback and forward active clamp converters, are frequently adopted due to their simplicity, reduced semiconductor count, and low cost. Simultaneously, interleaved topologies have emerged as a relevant solution for specific scenarios where compact design and high-power density are critical requirements. As a result, these topologies are also commonly used in residential cases and standalone solar PV systems, where the efficiency–cost ratio plays an important role in converter selection.

Regardless of the chosen topology and application, the performance of a power conversion stage is heavily influenced by the control algorithms and modulations employed. In bridge-based topologies, in addition to phase-shift techniques, efficiency can be further improved by adopting soft-switching techniques and zero-voltage/zero-current switching (ZVS/ZCS). Complementary to these strategies, advanced control techniques, such as model predictive control (MPC) and direct-quadrature-zero (DQ0) transformation, are widely explored to enhance stability and improve the dynamic response of RES-based systems. For NPC topologies, the use of space vector PWM (SVPWM) has proven to be particularly effective, notably in reducing THD and improving conversion efficiency, especially in high-power applications. Nevertheless, further efforts are required to augment the resilience of power electronics systems, particularly regarding fault tolerance, cybersecurity, switching redundancy, and self-healing algorithms. These advancements are vital to ensuring operational continuity in critical systems, including microgrids and power transmission and distribution grids.

5. Analysis of Power Semiconductor Technologies

In line with the ongoing technological advancements in the power semiconductor industry, particularly in WBG devices, isolated converters no longer necessitate the utilization of bulky components. In other words, as the switching frequency (f_{sw}) increases, the power density of the converters also rises. Thereby, power electronics solutions employing HFTs enable enhanced controllability and flexibility on the interfacing elements, while significantly reducing the overall volume and weight.

Owing to their superior material properties, WBG semiconductors doped with silicon carbide (SiC) or gallium nitride (GaN) have become increasingly prevalent in power electronics applications [157], particularly in high-frequency and high-power scenarios where traditional silicon (Si) devices are no longer viable. WBG devices exhibit a higher energy bandgap (E_g), improved stability, and reduced conduction losses compared to conventional Si semiconductors, as evidenced by their lower drain-source on-resistance ($R_{DS(on)}$) [158,159]. Nonetheless, the increase in E_g also results in a higher electric breakdown field (E_B) [160,161]. Consequently, a larger E_B magnitude enables WBG devices to achieve higher speed under elevated temperature and drain-source voltage (V_{DS}) conditions. Therefore, SiC and GaN semiconductors have become, respectively, attractive for high-power and HF applications [162–164].

As observed in Figure 25a, the use of SiC and GaN semiconductors leads to an extended voltage operating range and enhanced device speed, thereby mitigating the significant limitations of Si doping technology. Furthermore, due to the reduced required

charge for switching between turn-on and turn-off states in WBG semiconductors, the switching losses, even at high frequencies, are notably diminished compared to Si devices. However, as highlighted in [165], the long-term reliability of WBG devices is intrinsically linked to the performance of a given power electronics system. Considering the relatively reduced technological maturity of WBG devices, as well as the operating conditions they are subjected to, this topic still demands study and characterization. Critical challenges include high thermal stress, encapsulation degradation, and bond wire failures. Additionally, EMI mitigation mechanisms and the need for robust gate drivers impose additional constraints on WBG device adoption. Addressing these challenges, e.g., the development of failure prevention mechanisms at the semiconductor level, requires the study of different packaging approaches and investigation of high-current avalanche robustness.

Given the critical role of SiC and GaN devices on high-switching-frequency (f_{sw}) applications, it is crucial to subject these semiconductors to demanding testing under extreme operating conditions. Several reliability tests are explored in the literature, aiming to assess performance and longevity. The major focus lies on key stress factors that impact f_{sw}, thermal stability, and degradation. Among the methodologies, the high humidity, high temperature, reverse bias (H^3TRB) test stands out, particularly in applications where isolation and packaging integrity are critical [166]. Moreover, avalanche capability testing is fundamental for assessing semiconductor robustness against transient overvoltages [167], while radiation reliability and neutron radiation hardness testing ensure performance consistency [168]. On the other hand, backside laser testing allows us to identify weak points at the junction level [169]. Lastly, double-pulse testing plays a pivotal role in analyzing switching behavior, particularly in response to threshold voltage shifts, dynamic $R_{DS(on)}$ variations, and temperature deviations [170].

In [171], a characterization model for SiC MOSFETs was presented for study under various operating conditions. The main objective was to obtain concrete insights into nonlinear interelectrode capacitances, switching transitions, losses under both hard- and soft-switching conditions, and device-capacitance losses. To this end, a setup with multiple current-probe methods was developed, where three SiC MOSFETs (600 V, 900 V, and 1200 V) were subjected to different conditions. The results showed that semiconductors with higher V_{DS} have lower on-state resistance and smaller interelectrode capacitance compared to the 600 V devices. Consequently, both switching transients and losses are reduced.

To further enhance reliability, the packaging of WBG devices plays a pivotal role. Specifically, methods aimed at reducing on-state resistance need to be developed, as demonstrated by technologies like direct-cooled power modules with liquid [172] and double-sided direct cooling [173]. Additionally, modules with ultralow on-resistance can also be employed, as proposed in [174]. However, to effectively increase reliability and thermal response, suitable ceramic materials should also be selected for the substrate.

In the case of GaN-dopped WBG devices, this issue becomes even more prominent due to the adoption of higher f_{sw}. As crucial measures to enhance reliability, emphasis should be placed on reducing parasitic capacitances during layout design and utilizing magnetic materials with variable-width winding structures to mitigate core and winding losses resulting from skin effect [175]. Moreover, winding losses must also be duly considered in optimizing the performance of power electronics systems. To achieve this, over the past years, the use of planar transformers has gained significant importance, particularly in lower power and HF applications [176,177].

As highlighted in [178], to estimate the lifetime of each semiconductor module, the Coffin–Manson–Arrhenius formula is commonly employed:

$$N_f = b_1 \, \Delta T^{-\alpha} \, e^{\frac{E_a}{k_B T_{jm}}} \tag{2}$$

Here, the number of life cycles to failure, N_f, is determined based on the average operating temperature, T_{jm}, and the amplitude of thermal cycles, ΔT_j. Additionally, k_B corresponds to the Boltzmann constant, while the coefficients b_1, α, and E_a are dependent on the application scenario and operating conditions.

In this context, an extensive study regarding the reliability of WBG semiconductors under various operation scenarios was conducted in [179]. As an important feature, it mentioned the use of physics-of-failure models to accurately assess their reliability. These models encompass variations to evaluate time-dependent dielectric breakdown, stress–strain, and thermal cycling. The primary conclusion drawn from this article emphasizes the imperative need to transition to power electronics solutions based on WBG devices. Additionally, the repercussions stemming from the challenges of developing devices with enhanced characteristics in bond wires, solders, substrates, and encapsulants are highlighted. As a consequence, WBG devices are limited to an operating temperature of 175 °C, which is still far from sufficient to fully harness their potential.

For the aforementioned reasons, the selection of the semiconductor doping material is highly dependent on the specific power electronics application and its complementary characteristics. SiC technology, for instance, is notorious for its high breakdown voltage ($V_{BR(DSS)}$) and capability to operate at high temperatures and voltages, i.e., exhibiting superior thermal conductivity (k_{th}) compared to other commonly studied technologies [180–182]. However, as depicted in Figure 25b and detailed in Table 3, WBG SiC devices have lower electron mobility (μ_e), which may potentially result in slower semiconductor operation. However, this situation is primarily accentuated in low-voltage scenarios, in addition to other parameters that actively compensate for this negative effect. These parameters include the reduced reverse recovery time (t_{rr}) of the semiconductor's internal diode, low $R_{DS(on)}$, high electron saturation velocity (V_{nsat}), and enhanced E_g [183,184].

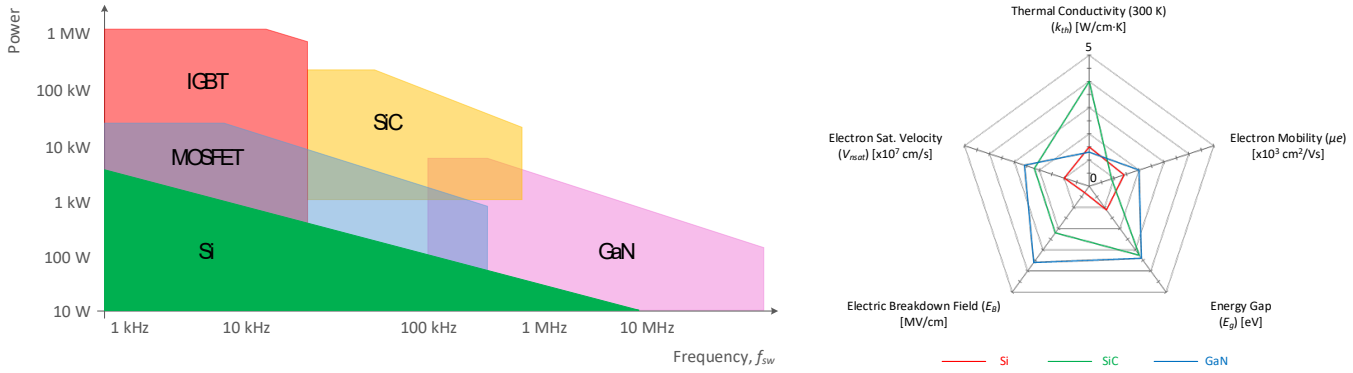

(**a**) (**b**)

Figure 25. Comparison between different semiconductor technologies (Si, SiC, and GaN) regarding the following: (**a**) operating power and switching frequency (f_{sw}) range and (**b**) electrical properties.

GaN doping processes, on the other hand, represent a relatively recent and less mature technology, which explains their limited suitability in high-power scenarios [185]. Notwithstanding, similar to SiC devices, GaN semiconductors exhibit low $R_{DS(on)}$ values, but, on the contrary, lower k_{th}, thus indicating a reduced adequacy to dissipate heat. Therefore, in low-current and high-f_{sw} scenarios, GaN semiconductors demonstrate higher efficiency compared to SiC technology [186]. This improved performance can be attributed to their reduced switching losses and high values of E_B and μ_e, which, in turn, allow for a smaller-sized switching device [187]. Additionally, the higher values of μ_e, V_{nsat}, and E_g, coupled with lower internal capacitances, enable WBG GaN semiconductors to achieve faster switching transients, making them highly suitable for high-f_{sw} application [188].

Table 3. Comparison of key electrical and thermal properties of silicon (Si), silicon carbide (SiC), and gallium nitride (GaN) semiconductors.

Property	Si Devices	SiC Devices	GaN Devices
Energy Bandgap (E_g) [eV]	1.1	3.3	3.4
Electric Breakdown Field (E_B) [MV/cm]	0.3	2.8	3.3
Thermal Conductivity (k_{th}) [W/cm·K]	1.5	3.9	1.3
Electron Mobility (μ_e) [$\times 10^3$ cm^2/V·s]	1.3	0.9	2.0
Electron Saturation Velocity (V_{nsat}) [$\times 10^7$ cm/s]	1.0	2.2	2.6
Drain-Source On-Resistance ($R_{DS(on)}$)	High	Low	Very Low
Switching Losses	High	Low	Very Low
Maximum Operating Temperature [°C]	150	175–200	175

Summarizing, based on the analysis of both the images in Figure 25, the use of GaN semiconductors is recommended over SiC when higher speed is required. On the other hand, SiC technology is considered more efficient for power electronics scenarios that require higher voltage and temperature operation. Both scenarios are of utmost importance regarding the implementation of isolated DC–DC converters. Consequently, in line with the premises associated with future smart grids and RES-based systems, these topologies must be endowed with higher power density (increased speed) and the ability to operate at elevated temperatures. More importantly, such behavior is only ensured with the selection of appropriate topologies, relevant modulation techniques, and, as expected, WBG switching devices.

As a practical example, in microinverter configurations, considering the mounting location of the interface system, it is pertinent to exhibit high power density and, at the same time, efficiently dissipate heat. From another perspective, in high-power scenarios, it is expected that the semiconductors will be subjected to higher stress, necessitating improved solar or wind energy conversion efficiency. Nevertheless, beyond their application in RES-based generation technologies, WBG devices also play an equally important role in various application scenarios, such as power systems interfacing with energy storage elements, EV charging stations, and power transmission and distribution, among others.

6. Conclusions

The primordial objective of this review paper is to establish an extensive but accurate study of different isolated DC–DC converters for power generation systems based on renewable energy sources (RESs). Alongside exploring various topologies and arrangements for the power converters, this review also encompasses the possible architectures and connection schemes for interfacing RES-based systems with the utility grid. Furthermore, the analysis has been extended to include emerging technologies and the current deployment scenarios of these converters.

Therefore, a concise yet pertinent analysis has been carried out to determine the most suitable switching power devices for the interface systems. To increase the power density of DC–DC converters utilizing high-frequency transformers (HFTs), there has been considerable interest in employing wide-bandgap (WBG) devices doped with silicon carbide (SiC) or gallium nitride (GaN), with particular prominence in applications such as solid-state transformers (SSTs). SiC semiconductors are strongly suitable for high-power applications due to their superior thermal conductivity, enabling efficient heat dissipation. However, although they are also applicable for high-frequency (HF) switching, they do not possess the same speed characteristics as GaN devices. On the downside, GaN technology is not yet fully suitable for high-power solutions and still demonstrates relatively lower technological maturity.

Although the selection of active semiconductors is a critical step in converter design, the converter's topology is arguably the characteristic of utmost importance. Isolated DC–DC converters can be categorized not only based on their power handling capability but also considering their scalability, flexibility, modularity, efficiency, cost, and reliability. In addition, they enhance immunity to noise and interference, fault tolerance, and most importantly, ease of voltage conversion.

As expected, multilevel topologies offer enhanced conversion efficiency compared to conventional ones. However, both half-bridge and full-bridge configurations also exhibit highly satisfactory efficiency indicators, which justifies their frequent use in a broader scenario. In addition, these topologies provide considerable technological maturity, thus facilitating the implementation of suitable and innovative modulation techniques. Nevertheless, in high- and very-high-power solutions, multilevel converters, particularly modular multilevel converters (MMCs), are the preferred option due to their capability to distribute a certain voltage and/or current across a larger number of active semiconductors. This scenario is equally observed when multiple converters are interconnected in parallel or cascade configurations, highlighting the significance of modularity and scalability.

Therefore, the selection of each topology will primarily depend on the requirements of the power electronics solution and the specific application. When it comes to interfacing with RES-based generation systems, all the converter topologies discussed in this review paper are considered appropriate. However, certain topologies may be considered more suitable for specific generation technologies or different power levels, ranging from microinverters to large-scale power plants. Among all the isolated DC–DC converters, bridge-based topologies are widely considered as the most consensual due to their flexibility and technological maturity. Furthermore, when interconnected to form a dual active bridge (DAB) converter, the advantages are further accentuated, enabling enhanced scalability and modularity based on the power rating of the application.

Author Contributions: Conceptualization, S.C., V.M. and J.L.A.; methodology, S.C.; validation, S.C. and V.M.; investigation, S.C. and V.M.; writing—original draft preparation, S.C.; writing—review and editing, S.C., V.M. and J.L.A.; supervision, V.M. and J.L.A.; funding acquisition, V.M. and J.L.A. All authors have read and agreed to the published version of the manuscript.

Funding: This paper was supported by the Alliance for the Energy Transition (56) co-financed by the Recovery and Resilience Plan (PRR) through the European Union. This work has been supported by FCT – Fundação para a Ciência e Tecnologia within the R&D Unit Project of ALGORITMI Centre.

Data Availability Statement: Not applicable.

Acknowledgments: Sergio Coelho is supported by the doctoral scholarship 2021.08965.BD, granted by FCT—Fundação para a Ciência e Tecnologia.

Conflicts of Interest: The authors declare no conflicts of interest.

References

1. IEA. *World Energy Outlook 2024*; IEA: Paris, France, 2024. Available online: https://www.iea.org/reports/world-energy-outlook-2024 (accessed on 23 February 2025).
2. Ritchie, H.; Rosado, P.; Roser, M. CO_2 and Greenhouse Gas Emissions. *Our World in Data*. December 2023. Available online: https://ourworldindata.org/co2-and-greenhouse-gas-emissions (accessed on 5 August 2024).
3. BP. bp Energy Outlook: 2024 Edition. July 2024. Available online: https://www.bp.com/en/global/corporate/energy-economics/energy-outlook.html (accessed on 23 February 2025).
4. Dröge, S.; Wissenschaft, S. *The Paris Agreement 2015: Turning Point for the International Climate Regime*; Stiftung Wissenschaft und Politik (SWP): Berlin, Germany, 2016.
5. Sanguesa, J.A.; Torres-Sanz, V.; Garrido, P.; Martinez, F.J.; Marquez-Barja, J.M. A Review on Electric Vehicles: Technologies and Challenges. *Smart Cities* **2021**, *4*, 372–404. [CrossRef]

6. Pasha, J.; Li, B.; Elmi, Z.; Fathollahi-Fard, A.M.; Lau, Y.; Roshani, A.; Kawasaki, T.; Dulebenets, M.A. Electric vehicle scheduling: State of the art, critical challenges, and future research opportunities. *J. Ind. Inf. Integr.* **2024**, *38*, 100561. [CrossRef]
7. Jiang, F.; Yuan, X.; Hu, L.; Xie, G.; Zhang, Z.; Li, X.; Hu, J.; Wang, C.; Wang, H. A comprehensive review of energy storage technology development and application for pure electric vehicles. *J. Energy Storage* **2024**, *86*, 111159. [CrossRef]
8. Ourahou, M.; Ayrir, W.; El Hassouni, B.; Haddi, A. Review on Smart Grid Control and Reliability in Presence of Renewable Energies: Challenges and Prospects. *Math. Comput. Simul.* **2020**, *167*, 19–31. [CrossRef]
9. Al-Shetwi, A.Q.; Hannan, M.A.; Jern, K.P.; Mansur, M.; Mahlia, T.M.I. Grid-Connected Renewable Energy Sources: Review of the Recent Integration Requirements and Control Methods. *J. Clean. Prod.* **2020**, *253*, 119831. [CrossRef]
10. Khalid, M. Smart grids and renewable energy systems: Perspectives and grid integration challenges. *Energy Strategy Rev.* **2024**, *51*, 101299. [CrossRef]
11. Alajrash, B.H.; Salem, M.; Swadi, M.; Senjyu, T.; Kamarol, M.; Motahhir, S. A comprehensive review of FACTS devices in modern power systems: Addressing power quality, optimal placement, and stability with renewable energy penetration. *Energy Rep.* **2024**, *11*, 5350–5371. [CrossRef]
12. Quizhpe, K.; Arévalo, P.; Ochoa-Correa, D.; Villa-Ávila, E. Optimizing Microgrid Planning for Renewable Integration in Power Systems: A Comprehensive Review. *Electronics* **2024**, *13*, 3620. [CrossRef]
13. Malinowski, M.; Leon, J.I.; Abu-Rub, H. Solar Photovoltaic and Thermal Energy Systems: Current Technology and Future Trends. *Proc. IEEE* **2017**, *105*, 2132–2146. [CrossRef]
14. Zia, M.F.; Elbouchikhi, E.; Benbouzid, M. Microgrids Energy Management Systems: A Critical Review on Methods, Solutions, and Prospects. *Appl. Energy* **2018**, *222*, 1033–1055. [CrossRef]
15. Wei, T.; Cervone, A.; Dujic, D. Active Power Decoupling for Single-Phase Input–Series–Output–Parallel Solid-State Transformers. *IEEE Trans. Power Electron.* **2024**, *39*, 5636–5648. [CrossRef]
16. Shi, H.; Wen, H.; Hu, Y.; Yang, Y.; Wang, Y. Efficiency Optimization of DC Solid-State Transformer for Photovoltaic Power Systems. *IEEE Trans. Ind. Electron.* **2020**, *67*, 3583–3595. [CrossRef]
17. Hashemzadeh, S.M.; Al-Hitmi, M.A.; Islam, S.; Iqbal, A.; Aghaei, H.; Hosseini, S.H.; Babaei, E. A high voltage gain solid-state transformer for integration of renewable energy and AC sources. *Sci. Rep.* **2024**, *14*, 25471. [CrossRef] [PubMed]
18. Raghavendra, K.V.G.; Zeb, K.; Muthusamy, A.; Krishna, T.N.V.; Kumar, S.V.S.V.P.; Kim, D.-H.; Kim, M.-S.; Cho, H.-G.; Kim, H.-J. A Comprehensive Review of DC–DC Converter Topologies and Modulation Strategies with Recent Advances in Solar Photovoltaic Systems. *Electronics* **2019**, *9*, 31. [CrossRef]
19. Blaabjerg, F.; Ma, K.; Yang, Y. Power Electronics for Renewable Energy Systems—Status and Trends. In Proceedings of the CIPS 2014; 8th International Conference on Integrated Power Electronics Systems, Nuremberg, Germany, 25–27 February 2014; pp. 1–11. Available online: https://ieeexplore.ieee.org/document/6776841/?arnumber=6776841 (accessed on 5 August 2024).
20. Kabalcı, E. Review on Novel Single-Phase Grid-Connected Solar Inverters: Circuits and Control Methods. *Sol. Energy* **2020**, *198*, 247–274. [CrossRef]
21. Vakacharla, V.R.; Gnana, K.; Xuewei, P.; Narasimaharaju, B.L.; Bhukya, M.; Banerjee, A.; Sharma, R.; Rathore, A.K. State-of-the-art power electronics systems for solar-to-grid integration. *Sol. Energy* **2020**, *210*, 128–148. [CrossRef]
22. Bell, B.; Hari, A. Topology Key to Power Density in Isolated DC-DC Converters. Available online: https://www.electronicdesign.com/technologies/power/power-supply/dc-dc-converters/article/21192993/topology-key-to-power-density-in-isolated-dc-dc-converters (accessed on 5 August 2024).
23. Sutikno, T.; Samosir, A.S.; Aprilianto, R.A.; Purnama, H.S.; Arsadiando, W.; Padmanaban, S. Advanced DC–DC Converter Topologies for Solar Energy Harvesting Applications: A Review. *Clean Energy* **2023**, *7*, 555–570. [CrossRef]
24. Bhuiyan, M.A.; Zhang, Q.; Khare, V.; Mikhaylov, A.; Pinter, G.; Huang, X. Renewable Energy Consumption and Economic Growth Nexus—A Systematic Literature Review. *Front. Environ. Sci.* **2022**, *10*, 878394. [CrossRef]
25. Ntanos, S.; Skordoulis, M.; Kyriakopoulos, G.; Arabatzis, G.; Chalikias, M.; Galatsidas, S.; Batzios, A.; Katsarou, A. Renewable Energy and Economic Growth: Evidence from European Countries. *Sustainability* **2018**, *10*, 2626. [CrossRef]
26. Filimonova, I.V.; Nemov, V.Y.; Komarova, A.V.; Mishenin, M.V.; Kozhevin, V.D. Relationship of renewable energy consumption to economic, environmental and institutional factors in Europe. *Energy Rep.* **2021**, *7*, 358–365. [CrossRef]
27. Elalfy, D.A.; Gouda, E.; Kotb, M.F.; Bureš, V.; Sedhom, B.E. Comprehensive review of energy storage systems technologies, objectives, challenges, and future trends. *Energy Strategy Rev.* **2024**, *54*, 101482. [CrossRef]
28. Zhang, Z.; Li, Z.; Kazmierkowski, M.P.; Rodriguez, J.; Kennel, R. Robust Predictive Control of Three-Level NPC Back-to-Back Power Converter PMSG Wind Turbine Systems with Revised Predictions. *IEEE Trans. Power Electron.* **2018**, *33*, 9588–9598. [CrossRef]
29. Yesudhas, A.A.; Lee, S.R.; Jeong, J.H.; Joo, Y.H. Performance enhancement using terminal synergetic approach-based back-to-back converter current control for grid connected PMVG wind energy conversion system under diverse operating conditions. *Comput. Electr. Eng.* **2025**, *122*, 109993. [CrossRef]

30. Guan, M. A Series-Connected Offshore Wind Farm Based on Modular Dual-Active-Bridge (DAB) Isolated DC–DC Converter. *IEEE Trans. Energy Convers.* **2019**, *34*, 1422–1431. [CrossRef]
31. Almeida, A.O.; Lopes, I.F.; Almeida, P.M.; Tomim, M.A.; Passos Filho, J.A.; Barbosa, P.G. Series-DC connection of Offshore wind generating units—Modeling, control and galvanic isolation. *Electr. Power Syst. Res.* **2021**, *195*, 107149. [CrossRef]
32. Liu, H.; Dahidah, M.S.A.; Yu, J.; Naayagi, R.T.; Armstrong, M. Design and Control of Unidirectional DC–DC Modular Multilevel Converter for Offshore DC Collection Point: Theoretical Analysis and Experimental Validation. *IEEE Trans. Power Electron.* **2019**, *34*, 5191–5208. [CrossRef]
33. Patel, H.; Bhawal, S.; Harikrishnan, P.; Hatua, K.; Bhattacharya, S. Three Stage Power Electronic Transformer Based MVAC Collection System and Its Control System Design for Offshore Wind Power Generation Mills. *IEEE Trans. Energy Convers.* **2024**, *39*, 2216–2229. [CrossRef]
34. Syed, I.; Khadkikar, V. Replacing the Grid Interface Transformer in Wind Energy Conversion System with Solid-State Transformer. *IEEE Trans. Power Syst.* **2017**, *32*, 2152–2160. [CrossRef]
35. Aragon-Aviles, S.; Trivedi, A.; Williamson, S.S. Smart Power Electronics–Based Solutions to Interface Solar-Photovoltaics (PV), Smart Grid, and Electrified Transportation: State-of-the-Art and Future Prospects. *Appl. Sci.* **2020**, *10*, 4988. [CrossRef]
36. Carrasco, J.M.; Franquelo, L.G.; Bialasiewicz, J.T.; Galvan, E.; PortilloGuisado, R.C.; Prats, M.A.M.; Leon, J.I.; Moreno-Alfonso, N. Power-Electronic Systems for the Grid Integration of Renewable Energy Sources: A Survey. *IEEE Trans. Ind. Electron.* **2006**, *53*, 1002–1016. [CrossRef]
37. Cabrera-Tobar, A.; Bullich-Massagué, E.; Aragüés-Peñalba, M.; Gomis-Bellmunt, O. Topologies for large scale photovoltaic power plants. *Renew. Sustain. Energy Rev.* **2016**, *59*, 309–319. [CrossRef]
38. Lucia, U. Overview on fuel cells. *Renew. Sustain. Energy Rev.* **2014**, *30*, 164–169. [CrossRef]
39. Abdelkareem, M.A.; Elsaid, K.; Wilberforce, T.; Kamil, M.; Sayed, E.T.; Olabi, A. Environmental aspects of fuel cells: A review. *Sci. Total Environ.* **2021**, *752*, 141803. [CrossRef]
40. Sharaf, O.Z.; Orhan, M.F. An Overview of Fuel Cell Technology: Fundamentals and Applications. *Renew. Sustain. Energy Rev.* **2014**, *32*, 810–853. [CrossRef]
41. Mousa, H.H.H.; Youssef, A.-R.; Mohamed, E.E.M. State of the art perturb and observe MPPT algorithms based wind energy conversion systems: A technology review. *Int. J. Electr. Power Energy Syst.* **2021**, *126*, 106598. [CrossRef]
42. Büyük, M.; İnci, M. Improved drift-free P&O MPPT method to enhance energy harvesting capability for dynamic operating conditions of fuel cells. *Energy* **2023**, *267*, 126543. [CrossRef]
43. Motahhir, S.; El Hammoumi, A.; El Ghzizal, A. The most used MPPT algorithms: Review and the suitable low-cost embedded board for each algorithm. *J. Clean. Prod.* **2020**, *246*, 118983. [CrossRef]
44. Sarvi, M.; Azadian, A. A Comprehensive Review and Classified Comparison of MPPT Algorithms in PV Systems. *Energy Syst.* **2022**, *13*, 281–320. [CrossRef]
45. İnci, M.; Türksoy, Ö. Review of fuel cells to grid interface: Configurations, technical challenges and trends. *J. Clean. Prod.* **2019**, *213*, 1353–1370. [CrossRef]
46. Zhang, Z.; Pittini, R.; Andersen, M.A.E.; Thomsena, O.C. A Review and Design of Power Electronics Converters for Fuel Cell Hybrid System Applications. *Energy Procedia* **2012**, *20*, 301–310. [CrossRef]
47. Wang, B.; Xian, L.; Kanamarlapudi, V.R.K.; Tseng, K.J.; Ukil, A.; Gooi, H.B. A Digital Method of Power-Sharing and Cross-Regulation Suppression for Single-Inductor Multiple-Input Multiple-Output DC–DC Converter. *IEEE Trans. Ind. Electron.* **2017**, *64*, 2836–2847. [CrossRef]
48. Latorre, A.; Soeiro, T.B.; Fan, X.; Geertsma, R.; Popov, M.; Polinder, H. Pole-to-Pole Short-Circuit Categorization for Protection Strategies in Primary Shipboard DC Systems. *IEEE Open J. Ind. Electron. Soc.* **2024**, *5*, 596–615. [CrossRef]
49. Li, C.; Gole, A.M.; Zhao, C. A Fast DC Fault Detection Method Using DC Reactor Voltages in HVdc Grids. *IEEE Trans. Power Delivery* **2018**, *33*, 2254–2264. [CrossRef]
50. Nguyen, T.H.; Hosani, K.A.; Moursi, M.S.E.; Blaabjerg, F. An Overview of Modular Multilevel Converters in HVDC Transmission Systems with STATCOM Operation During Pole-to-Pole DC Short Circuits. *IEEE Trans. Power Electron.* **2019**, *34*, 4137–4160. [CrossRef]
51. Xiang, W.; Yang, S.; Adam, G.P.; Zhang, H.; Zuo, W.; Wen, J. DC Fault Protection Algorithms of MMC-HVDC Grids: Fault Analysis, Methodologies, Experimental Validations, and Future Trends. *IEEE Trans. Power Electron.* **2021**, *36*, 11245–11264. [CrossRef]
52. Li, R.; Xu, L. Review of DC fault protection for HVDC grids. *WIREs Energy Environ.* **2018**, *7*, e278. [CrossRef]
53. Muniappan, M. A Comprehensive Review of DC Fault Protection Methods in HVDC Transmission Systems. *Prot. Control Mod. Power Syst.* **2021**, *6*, 1. [CrossRef]
54. Monteiro, V.; Pedrosa, D.; Coelho, S.; Sousa, T.; Machado, L.; Afonso, J.L. A Novel Multilevel Solid-State Transformer for Hybrid Power Grids. In Proceedings of the 2021 International Conference on Smart Energy Systems and Technologies (SEST), Vaasa, Finland, 6–8 September 2021; pp. 1–6.

55. Gulzar, M.M.; Iqbal, M.; Shahzad, S.; Muqeet, H.A.; Shahzad, M.; Hussain, M.M. Load Frequency Control (LFC) Strategies in Renewable Energy-Based Hybrid Power Systems: A Review. *Energies* **2022**, *15*, 3488. [CrossRef]
56. Gorji, S.A.; Sahebi, H.G.; Ektesabi, M.; Rad, A.B. Topologies and Control Schemes of Bidirectional DC–DC Power Converters: An Overview. *IEEE Access* **2019**, *7*, 117997–118019. [CrossRef]
57. Lu, Z.; Xu, G.; Su, M.; Liao, Y.; Liu, Y.; Sun, Y. Stability Analysis and Design of Common Phase Shift Control for Input-Series Output-Parallel Dual Active Bridge with Consideration of Dead-Time Effect. *IEEE J. Emerg. Sel. Topics Power Electron.* **2022**, *10*, 7721–7732. [CrossRef]
58. Chen, T.; Yu, R.; Huang, A.Q. A Bidirectional Isolated Dual-Phase-Shift Variable-Frequency Series Resonant Dual-Active-Bridge GaN AC–DC Converter. *IEEE Trans. Ind. Electron.* **2023**, *70*, 3315–3325. [CrossRef]
59. Krismer, F.; Kolar, J.W. Accurate Power Loss Model Derivation of a High-Current Dual Active Bridge Converter for an Automotive Application. *IEEE Trans. Ind. Electron.* **2010**, *57*, 881–891. [CrossRef]
60. Rezaei, M.A.; Lee, K.-J.; Huang, A.Q. A High-Efficiency Flyback Micro-inverter With a New Adaptive Snubber for Photovoltaic Applications. *IEEE Trans. Power Electron.* **2016**, *31*, 318–327. [CrossRef]
61. Falconar, N.; Beyragh, D.S.; Pahlevani, M. An Adaptive Sensorless Control Technique for a Flyback-Type Solar Tile Microinverter. *IEEE Trans. Power Electron.* **2020**, *35*, 13554–13562. [CrossRef]
62. Padhee, P.K.; Sekhar, P.C. Isolated Multi-Output Power Supply Based on Flyback Converter. In Proceedings of the 2023 International Conference on Power Electronics and Energy (ICPEE), Bhubaneswar, India, 3–5 January 2023; pp. 1–6.
63. Zengin, S.; Deveci, F.; Boztepe, M. Decoupling Capacitor Selection in DCM Flyback PV Microinverters Considering Harmonic Distortion. *IEEE Trans. Power Electron.* **2013**, *28*, 816–825. [CrossRef]
64. Zhang, Z.; He, X.-F.; Liu, Y.-F. An Optimal Control Method for Photovoltaic Grid-Tied-Interleaved Flyback Microinverters to Achieve High Efficiency in Wide Load Range. *IEEE Trans. Power Electron.* **2013**, *28*, 5074–5087. [CrossRef]
65. Chen, Z.; Shen, L.; Wu, Y. An Improved Interleaved Flyback Converter with Reduced Voltage Stress and Current Auto-sharing. *J. Electr. Eng. Technol.* **2024**, *19*, 2251–2263. [CrossRef]
66. Sukesh, N.; Pahlevaninezhad, M.; Jain, P.K. Analysis and Implementation of a Single-Stage Flyback PV Microinverter with Soft Switching. *IEEE Trans. Ind. Electron.* **2014**, *61*, 1819–1833. [CrossRef]
67. Lodh, T.; Pragallapati, N.; Agarwal, V. Novel Control Scheme for an Interleaved Flyback Converter Based Solar PV Microinverter to Achieve High Efficiency. *IEEE Trans. Ind. Appl.* **2018**, *54*, 3473–3482. [CrossRef]
68. Abramovitz, A.; Cheng, T.; Smedley, K. Analysis and Design of Forward Converter with Energy Regenerative Snubber. *IEEE Trans. Power Electron.* **2010**, *25*, 667–676. [CrossRef]
69. Oluwasogo, E.S.; Konrath, J.P. An accurate small-signal model of a low-side active clamp forward converter and stability assessment in hard- and soft-switching operations. *IET Power Electron.* **2024**, *17*, 2956–2970. [CrossRef]
70. De Aragao Filho, W.C.P.; Barbi, I. A comparison between two current-fed push-pull DC-DC converters-analysis, design and experimentation. In Proceedings of the Proceedings of Intelec'96—International Telecommunications Energy Conference, Boston, MA, USA, 6–10 October 1996; pp. 313–320.
71. Díaz, M.; Muñoz, J.; Rivera, M.; Rohten, J. A Comprehensive Control Strategy for a Push–Pull Microinverter Connected to the Grid. *Energies* **2023**, *16*, 3196. [CrossRef]
72. Bal, S.; Rathore, A.; Srinivasan, D. Naturally Clamped Snubberless Soft-Switching Bidirectional Current-Fed Three-Phase Push-Pull DC/DC Converter for DC Micro-Grid Application. *IEEE Trans. Ind. Appl.* **2015**, *52*, 1577–1587. [CrossRef]
73. Munoz, J.; Diaz, M.; Rivera, M.; Dekka, A. Push-Pull Microinverter based on a Sub-modular Structure. In Proceedings of the 2022 International Symposium on Power Electronics, Electrical Drives, Automation and Motion (SPEEDAM), Sorrento, Italy, 22–24 June 2022; pp. 883–888.
74. Liu, K.-H.; Lee, F.C. Zero-Voltage Switching Technique in DC/DC Converters. In Proceedings of the 1986 17th Annual IEEE Power Electronics Specialists Conference, Vancouver, BC, Canada, 23–27 June 1986; pp. 58–70.
75. Litrán, S.P.; Durán, E.; Semião, J.; Díaz-Martín, C. Multiple-Output DC–DC Converters: Applications and Solutions. *Electronics* **2022**, *11*, 1258. [CrossRef]
76. Wu, H.; Xu, P.; Hu, H.; Zhou, Z.; Xing, Y. Multiport Converters Based on Integration of Full-Bridge and Bidirectional DC–DC Topologies for Renewable Generation Systems. *IEEE Trans. Ind. Electron.* **2014**, *61*, 856–869. [CrossRef]
77. Bottion, A.J.B.; Barbi, I. Input-Series and Output-Series Connected Modular Output Capacitor Full-Bridge PWM DC–DC Converter. *IEEE Trans. Ind. Electron.* **2015**, *62*, 6213–6221. [CrossRef]
78. Shu, L.; Chen, W.; Li, R.; Zhang, K.; Deng, F.; Yuan, Y.; Wang, T. A Three-Phase Triple-Voltage Dual-Active-Bridge Converter for Medium Voltage DC Transformer to Reduce the Number of Submodules. *IEEE Trans. Power Electron.* **2020**, *35*, 11574–11588. [CrossRef]
79. Majmunovic, B.; Mukherjee, S.; Martin, T.; Mallik, R.; Dutta, S.; Seo, G.-S.; Johnson, B.; Maksimovic, D. 1 kV, 10-kW SiC-Based Quadruple Active Bridge DCX Stage in a DC to Three-Phase AC Module for Medium-Voltage Grid Integration. *IEEE Trans. Power Electron.* **2022**, *37*, 14631–14646. [CrossRef]

80. Arias, M.; Lamar, D.G.; Linera, F.F.; Balocco, D.; Diallo, A.A.; Sebastián, J. Design of a Soft-Switching Asymmetrical Half-Bridge Converter as Second Stage of an LED Driver for Street Lighting Application. *IEEE Trans. Power Electron.* **2012**, *27*, 1608–1621. [CrossRef]
81. Tuan, C.A.; Takeshita, T. Analysis and Output Power Control of Unidirectional Secondary-Resonant Single-Active-Half-Bridge DC-DC Converter. *Energies* **2021**, *14*, 7432. [CrossRef]
82. Vasiladiotis, M.; Rufer, A. A Modular Multiport Power Electronic Transformer with Integrated Split Battery Energy Storage for Versatile Ultrafast EV Charging Stations. *IEEE Trans. Ind. Electron.* **2015**, *62*, 3213–3222. [CrossRef]
83. Schulz, M.; Ditze, S. Analysis and Experimental Verification of an Isolated Half-Bridge Bidirectional DC−DC Converter. *IEEE Trans. Power Electron.* **2022**, *37*, 5089–5106. [CrossRef]
84. Goudarzitaemeh, S.; Pahlevani, M. A Bidirectional DC–DC Converter with Direct Power Transfer. *IEEE Open J. Power Electron.* **2024**, *5*, 232–249. [CrossRef]
85. Wang, R.; Li, Y.; Sun, C.; Hu, S.; Li, X.; Chen, W.; Lv, G. Analysis and Verification of a Half-Dual Bridge Resonant Converter with Voltage Match Modulation. *Electronics* **2022**, *11*, 2675. [CrossRef]
86. Hyun, S.-W.; Lee, H.-J.; Shin, S.-C.; Lee, T.-K.; Won, C.-Y. New Power Conditioning System combined interleaved full-bridge converter with half-bridge inverter. In Proceedings of the 2013 IEEE International Symposium on Industrial Electronics, Taipei, Taiwan, 28–31 May 2013; pp. 1–6.
87. Sang, Y.; Junyent-Ferre, A.; Green, T.C. Operational Principles of Three-Phase Single Active Bridge DC/DC Converters Under Duty Cycle Control. *IEEE Trans. Power Electron.* **2020**, *35*, 8737–8750. [CrossRef]
88. Kheraluwala, M.N.; Gascoigne, R.W.; Divan, D.M.; Baumann, E.D. Performance characterization of a high-power dual active bridge DC-to-DC converter. *IEEE Trans. Ind. Appl.* **1992**, *28*, 1294–1301. [CrossRef]
89. Zhao, B.; Song, Q.; Liu, W.; Sun, Y. Overview of Dual-Active-Bridge Isolated Bidirectional DC–DC Converter for High-Frequency-Link Power-Conversion System. *IEEE Trans. Power Electron.* **2014**, *29*, 4091–4106. [CrossRef]
90. Sengupta, A.; Pereira, T.; Liserre, M. Design Optimization of Dual Active Bridge Converter for Supercapacitor Application. *IEEE Trans. Power Electron.* **2024**, *39*, 11544–11557. [CrossRef]
91. Xie, H.; Chen, X.; Ouyang, H.; Zhang, T.; Xie, R.; Zhang, Y. An Efficient Dual-Active-Bridge Converter for Wide Voltage Range by Switching Operating Modes with Different Transformer Equivalent Turns Ratios. *IEEE Trans. Power Electron.* **2024**, *39*, 9705–9716. [CrossRef]
92. Deepti, T.; Deepa, K.; Alexander Stonier, A.; Peter, G.; Anoop, A.; Shahila, D.F.D.; Ganji, V.; Jha, A. Analysis of Leakage Inductance Effect and Loss Calculation of DAB Using Single-Phase Shift Modulation Scheme. *IET Circuits Devices Syst.* **2025**, *2025*, 3536991. [CrossRef]
93. ElMenshawy, M.; Massoud, A. Medium-Voltage DC-DC Converter Topologies for Electric Bus Fast Charging Stations: State-of-the-Art Review. *Energies* **2022**, *15*, 5487. [CrossRef]
94. Rong, X.; Shek, J.K.H.; Macpherson, D.E. The study of different unidirectional input parallel output series connected DC-DC converters for wind farm based multi-connected DC system. *Int. Trans. Electr. Energy Syst.* **2021**, *31*, e12855. [CrossRef]
95. ElMenshawy, M.; Massoud, A. Modular Isolated DC-DC Converters for Ultra-Fast EV Chargers: A Generalized Modeling and Control Approach. *Energies* **2020**, *13*, 2540. [CrossRef]
96. Zhang, N.; Sutanto, D.; Muttaqi, K.M. A Review of Topologies of Three-Port DC–DC Converters for the Integration of Renewable Energy and Energy Storage System. *Renew. Sustain. Energy Rev.* **2016**, *56*, 388–401. [CrossRef]
97. Madhana, R.; Mani, G. Power enhancement methods of renewable energy resources using multiport DC-DC converter: A technical review. *Sustain. Comput. Inform. Syst.* **2022**, *35*, 100689. [CrossRef]
98. Naseem, N.; Cha, H. Quad-Active-Bridge Converter with Current Balancing Coupled Inductor for SST Application. *IEEE Trans. Power Electron.* **2021**, *36*, 12528–12539. [CrossRef]
99. Gong, S.; Li, X.; Han, J.; Sun, Y.; Xu, G.; Jiang, Y.; Huang, S. Sliding Mode Control-Based Decoupling Scheme for Quad-Active Bridge DC–DC Converter. *IEEE J. Emerg. Sel. Topics Power Electron.* **2022**, *10*, 1153–1164. [CrossRef]
100. Falcones, S.; Ayyanar, R.; Mao, X. A DC–DC Multiport-Converter-Based Solid-State Transformer Integrating Distributed Generation and Storage. *IEEE Trans. Power Electron.* **2013**, *28*, 2192–2203. [CrossRef]
101. Taylor, A.; Liu, G.; Bai, H.; Brown, A.; Johnson, P.M.; McAmmond, M. Multiple-Phase-Shift Control for a Dual Active Bridge to Secure Zero-Voltage Switching and Enhance Light-Load Performance. *IEEE Trans. Power Electron.* **2018**, *33*, 4584–4588. [CrossRef]
102. Kayaalp, I.; Demirdelen, T.; Koroglu, T.; Cuma, M.U.; Bayindir, K.C.; Tumay, M. Comparison of Different Phase-Shift Control Methods at Isolated Bidirectional DC-DC Converter. *Int. J. Appl. Math. Electron. Comput.* **2016**, *4*, 68. [CrossRef]
103. Coelho, S.; Sousa, T.J.C.; Monteiro, V.; Machado, L.; Afonso, J.L.; Couto, C. Comparative Analysis and Validation of Different Modulation Strategies for an Isolated DC-DC Dual Active Bridge Converter. In *Sustainable Energy for Smart Cities*; Afonso, J.L., Monteiro, V., Pinto, J.G., Eds.; Springer International Publishing: Cham, Switzerland, 2021; pp. 30–49.
104. Bu, Q.; Wen, H.; Shi, H.; Zhu, Y. A Comparative Review of High-Frequency Transient DC Bias Current Mitigation Strategies in Dual-Active-Bridge DC–DC Converters Under Phase-Shift Modulations. *IEEE Trans. Ind. Appl.* **2022**, *58*, 2166–2182. [CrossRef]

105. Bai, H.; Nie, Z.; Mi, C.C. Experimental Comparison of Traditional Phase-Shift, Dual-Phase-Shift, and Model-Based Control of Isolated Bidirectional DC–DC Converters. *IEEE Trans. Power Electron.* **2010**, *25*, 1444–1449. [CrossRef]
106. Shao, S.; Jiang, M.; Ye, W.; Li, Y.; Zhang, J.; Sheng, K. Optimal Phase-Shift Control to Minimize Reactive Power for a Dual Active Bridge DC–DC Converter. *IEEE Trans. Power Electron.* **2019**, *34*, 10193–10205. [CrossRef]
107. Akbar, S.M.; Hasan, A.; Watson, A.J.; Wheeler, P. Model Predictive Control with Triple Phase Shift Modulation for a Dual Active Bridge DC-DC Converter. *IEEE Access* **2021**, *9*, 98603–98614. [CrossRef]
108. Lin, F.; Zhang, X.; Li, X.; Sun, C.; Cai, W.; Zhang, Z. Automatic Triple Phase-Shift Modulation for DAB Converter with Minimized Power Loss. *IEEE Trans. Ind. Appl.* **2022**, *58*, 3840–3851. [CrossRef]
109. Gu, Q.; Yuan, L.; Nie, J.; Sun, J.; Zhao, Z. Current Stress Minimization of Dual-Active-Bridge DC–DC Converter Within the Whole Operating Range. *IEEE J. Emerg. Sel. Top. Power Electron.* **2019**, *7*, 129–142. [CrossRef]
110. Kaiwart, V.K.; Jamatia, A.; Chakrabarti, A.; Das, B.; Kasari, P.R.; Laskar, N. Modeling of Dual Active Bridge with Extended Phase Shift and Dual Phase Shift Modulation Technique using Reduced Order Model Method. In Proceedings of the 2023 Second International Conference on Electronics and Renewable Systems (ICEARS), Tuticorin, India, 2–4 March 2023; pp. 13–20.
111. Shi, H.; Wen, H.; Chen, J.; Hu, Y.; Jiang, L.; Chen, G.; Ma, J. Minimum-Backflow-Power Scheme of DAB-Based Solid-State Transformer with Extended-Phase-Shift Control. *IEEE Trans. Ind. Appl.* **2018**, *54*, 3483–3496. [CrossRef]
112. Morsali, P.; Dey, S.; Mallik, A.; Akturk, A. Switching Modulation Optimization for Efficiency Maximization in a Single-Stage Series Resonant DAB-Based DC–AC Converter. *IEEE J. Emerg. Sel. Top. Power Electron.* **2023**, *11*, 5454–5469. [CrossRef]
113. Liu, F.; Chen, Y.; Chen, X. Comprehensive Analysis of Three-Phase Three-Level LC-Type Resonant DC/DC Converter with Variable Frequency Control—Series Resonant Converter. *IEEE Trans. Power Electron.* **2017**, *32*, 5122–5131. [CrossRef]
114. Rocha, J.; Saghir, A.; Coelho, S.; Rego, G.; Afonso, J.L.; Monteiro, V. Design and Implementation of a DC–DC Resonant LLC Converter for Electric Vehicle Fast Chargers. *Energies* **2025**, *18*, 1099. [CrossRef]
115. Haga, H.; Kurokawa, F. Modulation Method of a Full-Bridge Three-Level LLC Resonant Converter for Battery Charger of Electrical Vehicles. *IEEE Trans. Power Electron.* **2017**, *32*, 2498–2507. [CrossRef]
116. Liu, C.; Liu, H.; Cai, G.; Cui, S.; Liu, H.; Yao, H. Novel Hybrid LLC Resonant and DAB Linear DC–DC Converter: Average Model and Experimental Verification. *IEEE Trans. Ind. Electron.* **2017**, *64*, 6970–6978. [CrossRef]
117. Pan, Y.; Yang, Y.; He, J.; Sangwongwanich, A.; Zhang, C.; Liu, Y.; Blaabjerg, F. A Dual-Loop Control to Ensure Fast and Stable Fault-Tolerant Operation of Series Resonant DAB Converters. *IEEE Trans. Power Electron.* **2020**, *35*, 10994–11012. [CrossRef]
118. Li, B.; Lee, F.C.; Li, Q.; Liu, Z. Bi-directional on-board charger architecture and control for achieving ultra-high efficiency with wide battery voltage range. In Proceedings of the 2017 IEEE Applied Power Electronics Conference and Exposition (APEC), Tampa, FL, USA, 26–30 March 2017; pp. 3688–3694.
119. James, L.D.; Teixeira, C.A.; Wilkinson, R.H.; McGrath, B.P.; Holmes, D.G.; Riedel, J. Adaptive Modulation of Resonant DAB Converters for Wide Range ZVS Operation with Minimum Reactive Circulating Power. *IEEE Trans. Ind. Appl.* **2022**, *58*, 7396–7407. [CrossRef]
120. Twiname, R.P.; Thrimawithana, D.J.; Madawala, U.K.; Baguley, C.A. A New Resonant Bidirectional DC–DC Converter Topology. *IEEE Trans. Power Electron.* **2014**, *29*, 4733–4740. [CrossRef]
121. Guo, Z.; Zhan, W.; Chen, Z. Single-Stage Isolated AC–DC Converter Based on LCL Resonant DAB Converters with Single-Loop Control. *IEEE Trans. Power Electron.* **2024**, *39*, 9305–9317. [CrossRef]
122. Ryu, M.-H.; Kim, H.-S.; Baek, J.-W.; Kim, H.-G.; Jung, J.-H. Effective Test Bed of 380-V DC Distribution System Using Isolated Power Converters. *IEEE Trans. Ind. Electron.* **2015**, *62*, 4525–4536. [CrossRef]
123. Safayatullah, M.; Elrais, M.T.; Ghosh, S.; Rezaii, R.; Batarseh, I. A Comprehensive Review of Power Converter Topologies and Control Methods for Electric Vehicle Fast Charging Applications. *IEEE Access* **2022**, *10*, 40753–40793. [CrossRef]
124. Song, W.; Zhong, M.; Luo, S.; Yang, S. Model Predictive Power Control for Bidirectional Series-Resonant Isolated DC–DC Converters with Fast Dynamic Response in Locomotive Traction System. *IEEE Trans. Transp. Electrific.* **2020**, *6*, 1326–1337. [CrossRef]
125. Chen, G.; Xu, N.; Yuan, L.; Humayun, M.; Khan, M.M. A DC-DC Center-Tapped Resonant Dual-Active Bridge with Two Modulation Techniques. *Electronics* **2020**, *9*, 1699. [CrossRef]
126. Wu, J.; Li, Y.; Sun, X.; Liu, F. A New Dual-Bridge Series Resonant DC–DC Converter with Dual Tank. *IEEE Trans. Power Electron.* **2018**, *33*, 3884–3897. [CrossRef]
127. Sun, X.; Shen, Y.; Li, W.; Wang, B.; Wang, L.; Li, X. Center-tapped transformer based bidirectional dc-dc converter with wide input voltage range. In Proceedings of the 2015 IEEE Energy Conversion Congress and Exposition (ECCE), Montreal, QC, Canada, 20–24 September 2015; pp. 5910–5917.
128. Roggia, L.; Costa, P.F.S. Comparative Analysis Between Integrated Full-Bridge-Forward and Dual Active Bridge DC–DC Converters. *Electron. Lett.* **2018**, *54*, 231–233. [CrossRef]

129. Zientarski, J.R.R.; Martins, M.L.D.S.; Pinheiro, J.R.; Hey, H.L. Series-Connected Partial-Power Converters Applied to PV Systems: A Design Approach Based on Step-Up/Down Voltage Regulation Range. *IEEE Trans. Power Electron.* **2018**, *33*, 7622–7633. [CrossRef]
130. Köse, H.; Aydemir, M.T. Design and implementation of a 22 kW full-bridge push–pull series partial power converter for stationary battery energy storage system with battery charger. *Meas. Control* **2020**, *53*, 1454–1464. [CrossRef]
131. Chen, J.; Nguyen, M.-K.; Yao, Z.; Wang, C.; Gao, L.; Hu, G. DC-DC Converters for Transportation Electrification: Topologies, Control, and Future Challenges. *IEEE Electrific. Mag.* **2021**, *9*, 10–22. [CrossRef]
132. Jou, H.-L.; Wu, K.-D.; Wu, J.-C.; Lin, Y.-Z.; Su, L.-W. Asymmetric isolated unidirectional multi-level DC-DC power converter. *Eng. Sci. Technol. Int. J.* **2019**, *22*, 894–898. [CrossRef]
133. Moonem, M.; Pechacek, C.; Hernandez, R.; Krishnaswami, H. Analysis of a Multilevel Dual Active Bridge (ML-DAB) DC-DC Converter Using Symmetric Modulation. *Electronics* **2015**, *4*, 239–260. [CrossRef]
134. Xuan, Y.; Yang, X.; Chen, W.; Liu, T.; Hao, X. A Novel NPC Dual-Active-Bridge Converter with Blocking Capacitor for Energy Storage System. *IEEE Trans. Power Electron.* **2019**, *34*, 10635–10649. [CrossRef]
135. Song, C.; Sangwongwanich, A.; Yang, Y.; Blaabjerg, F. Optimal Control of Multilevel DAB Converters for Soft-Switching and Minimum Current Stress. *IEEE Trans. Power Electron.* **2024**, *39*, 5707–5720. [CrossRef]
136. Wu, J.; Liu, D.; Wang, Y.; Pereira, T.; Liserre, M.; Chen, Z. Hybrid-Bridge-Based Dual-Active-Bridge Converter with an Asymmetric Active-Neutral-Point-Clamped Three-Level Bridge. *IEEE Trans. Circuits Syst. I Regul. Pap.* **2024**, *71*, 4873–4886. [CrossRef]
137. Feng, Z.; Wen, H.; Bu, Q.; Zhu, Y.; Han, X.; Zhou, J.; Lim, E.G.; Liu, W.; Hu, Y. Loss Balance and Transient DC-Bias Suppression Strategies in Three-Level DAB Converters Modulated with Five DoFs. *IEEE Trans. Power Electron.* **2023**, *38*, 8150–8164. [CrossRef]
138. Cao, H.; Lin, N.; Darvish, P.; Yang, Y.; Wang, Z.; Zhao, Y. Enhanced Triple Phase Shift Modulation Strategy for ANPC-DAB Converter to Extend Soft Switching Range. In Proceedings of the 2024 IEEE Applied Power Electronics Conference and Exposition (APEC), Long Beach, CA, USA, 25–29 February 2024; pp. 445–452.
139. Deng, Z.; Wang, G.; Wang, K.; Hao, Y. Analysis and Control of N-level Neutral-point Clamped Dual Active Bridge DC-DC Converter with Capacitor Voltage Balance. In Proceedings of the 2018 International Conference on Power System Technology (POWERCON), Guangzhou, China, 6–8 November 2018; pp. 2407–2413.
140. Liu, W.; Jin, H.; Yao, W.; Lu, Z. An Interleaved PWM Method with Better Voltage-Balancing Ability for Half-Bridge Three-Level DC/DC Converter. *IEEE Trans. Power Electron.* **2018**, *33*, 4594–4598. [CrossRef]
141. Tian, J.; Zhuo, C.; Wang, F.; Deng, H. An RMS Current Minimization Method for Three-Level ANPC-DAB-Based Distributed Energy Storage System with Full Operation ZVS. *IEEE J. Emerg. Sel. Top. Power Electron.* **2024**, *12*, 2388–2405. [CrossRef]
142. Guan, Q.-X.; Zhang, Y.; Zhao, H.-B.; Kang, Y. Optimized Switching Strategy for ANPC–DAB Converter Through Multiple Zero States. *IEEE Trans. Power Electron.* **2022**, *37*, 2885–2898. [CrossRef]
143. Zhao, B.; Song, Q.; Li, J.; Xu, X.; Liu, W. Comparative Analysis of Multilevel-High-Frequency-Link and Multilevel-DC-Link DC–DC Transformers Based on MMC and Dual-Active Bridge for MVDC Application. *IEEE Trans. Power Electron.* **2018**, *33*, 2035–2049. [CrossRef]
144. Sun, C.; Zhang, J.; Shi, G.; Cai, X. Inter-arm phase-shift modulation scheme for isolated modular multilevel DC-DC converter. In Proceedings of the 2016 IEEE 8th International Power Electronics and Motion Control Conference (IPEMC-ECCE Asia), Hefei, China, 22–26 May 2016; pp. 53–58.
145. Yadav, A.; Singh, S.N.; Das, S.P. Modular multi-level converter topologies: Present status and key challenges. In Proceedings of the 2017 4th IEEE Uttar Pradesh Section International Conference on Electrical, Computer and Electronics (UPCON), Mathura, India, 26–28 October 2017; pp. 280–288.
146. Sotoodeh, P.; Miller, R.D. A Single-Phase 5-Level Inverter with FACTS Capability using Modular Multi-Level Converter (MMC) Topology. In Proceedings of the 2013 International Electric Machines & Drives Conference, Chicago, IL, USA, 12–15 May 2013; pp. 1229–1234.
147. Zhang, L.; Zhao, Z.; Qin, J. Efficiency Optimization Design of DC-DC Solid State Transformer based on Modular Multilevel Converters. In Proceedings of the 2017 IEEE Energy Conversion Congress and Exposition (ECCE), Cincinnati, OH, USA, 1–5 October 2017; pp. 3508–3513.
148. Wang, Z.; Li, H.; Chu, Z.; Zhang, C.; Yang, Z.; Shao, T.; Hu, Y. A Review of EMI Research in Modular Multilevel Converter for HVDC Applications. *IEEE Trans. Power Electron.* **2022**, *37*, 14482–14498. [CrossRef]
149. Song, S.; Liu, J.; Chen, X. An MMC DC-Link Voltage Control Method Without Actual Voltage Measurement. *IEEE J. Emerg. Sel. Top. Power Electron.* **2022**, *10*, 5698–5708. [CrossRef]
150. Song, S.; Liu, J. Interpreting the Individual Capacitor Voltage Regulation Control of PSC-PWM MMC via Consensus Theory. *IEEE Access* **2019**, *7*, 66807–66820. [CrossRef]
151. Tavakoli, S.D.; Sanchez-Sanchez, E.; Prieto-Araujo, E.; Gomis-Bellmunt, O. DC Voltage Droop Control Design for MMC-Based Multiterminal HVDC Grids. *IEEE Trans. Power Deliv.* **2020**, *35*, 2414–2424. [CrossRef]

152. Ma, Z.; Gao, F.; Zhang, C.; Li, W.; Niu, D. Variable DC-Link Voltage Regulation of Single-Phase MMC Battery Energy-Storage System for Reducing Additional Charge Throughput. *IEEE Trans. Power Electron.* **2021**, *36*, 14267–14281. [CrossRef]
153. Lu, Z.; Lin, L.; Wang, X.; Xu, C. LLC-MMC Resonant DC-DC Converter: Modulation Method and Capacitor Voltage Balance Control Strategy. In Proceedings of the 2020 IEEE Applied Power Electronics Conference and Exposition (APEC), New Orleans, LA, USA, 15–19 March 2020; pp. 2056–2061.
154. Sun, P.; Tian, Y.; Pou, J.; Konstantinou, G. Beyond the MMC: Extended Modular Multilevel Converter Topologies and Applications. *IEEE Open J. Power Electron.* **2022**, *3*, 317–333. [CrossRef]
155. Ansari, J.A.; Liu, C.; Khan, S.A. MMC Based MTDC Grids: A Detailed Review on Issues and Challenges for Operation, Control and Protection Schemes. *IEEE Access* **2020**, *8*, 168154–168165. [CrossRef]
156. Jia, G.; Shi, B.; Li, M.; Chen, M.; Niu, F.; Tang, Y. Active Power Decoupling for Full-Bridge Submodules of a Modular Multilevel Converter. *IEEE Trans. Power Electron.* **2024**, *39*, 9752–9764. [CrossRef]
157. Prajapati, P.; Balamurugan, S. Leveraging GaN for DC-DC Power Modules for Efficient EVs: A Review. *IEEE Access* **2023**, *11*, 95874–95888. [CrossRef]
158. Nouketcha, F.; Lelis, A.; Green, R.; Cui, Y.; Darmody, C.; Goldsman, N. Detailed Study of Breakdown Voltage and Critical Field in Wide Bandgap Semiconductors. In Proceedings of the 2019 IEEE 7th Workshop on Wide Bandgap Power Devices and Applications (WiPDA), Raleigh, NC, USA, 29–31 October 2019; pp. 200–207.
159. Jones, E.A.; Wang, F.F.; Costinett, D. Review of Commercial GaN Power Devices and GaN-Based Converter Design Challenges. *IEEE J. Emerg. Sel. Topics Power Electron.* **2016**, *4*, 707–719. [CrossRef]
160. Slobodyan, O.; Flicker, J.; Dickerson, J.; Shoemaker, J.; Binder, A.; Smith, T.; Goodnick, S.; Kaplar, R.; Hollis, M. Analysis of the dependence of critical electric field on semiconductor bandgap. *J. Mater. Res.* **2022**, *37*, 849–865. [CrossRef]
161. Lophitis, N.; Arvanitopoulos, A.; Perkins, S.; Antoniou, M. TCAD Device Modelling and Simulation of Wide Bandgap Power Semiconductors. In *Disruptive Wide Bandgap Semiconductors, Related Technologies, and Their Applications*; Sharma, Y.K., Ed.; InTech: London, UK, 2018; ISBN 978-1-78923-668-2.
162. Baliga, B.J. Gallium nitride devices for power electronic applications. *Semicond. Sci. Technol.* **2013**, *28*, 074011. [CrossRef]
163. Jakka, V.N.; Nath, H.; Acharya, S.; Kadavelugu, A.; Madhusoodhanan, S.; Tripathi, A.; Patel, D.; Mainali, K.; Bhattacharya, S. Implementation of Flexible Large Power Transformers Using Modular Solid State Transformer Topologies Enabled by SiC Devices. In Proceedings of the 2019 IEEE Energy Conversion Congress and Exposition (ECCE), Baltimore, MD, USA, 29 September –3 October 2019; pp. 4619–4626.
164. Wang, F.; Ji, S. Benefits of high-voltage SiC-based power electronics in medium-voltage power-distribution grids. *Chin. J. Electr. Eng.* **2021**, *7*, 1–26. [CrossRef]
165. Iannaccone, G.; Sbrana, C.; Morelli, I.; Strangio, S. Power Electronics Based on Wide-Bandgap Semiconductors: Opportunities and Challenges. *IEEE Access* **2021**, *9*, 139446–139456. [CrossRef]
166. Rodriguez, J.A.; Tsoi, T.; Graves, D.; Bayne, S.B. Evaluation of GaN HEMTs in H3TRB Reliability Testing. *Electronics* **2022**, *11*, 1532. [CrossRef]
167. Zhong, K.; Sun, J.; Wang, Y.; Lyu, G.; Feng, S.; Chen, T.; Chen, K.J. Avalanche Capability of 650-V Normally-off GaN/SiC Cascode Power Device. In Proceedings of the 2021 33rd International Symposium on Power Semiconductor Devices and ICs (ISPSD), Nagoya, Japan, 30 May–3 June 2021; pp. 223–226.
168. Ahmed, M.; Kucukgok, B.; Yanguas-Gil, A.; Hryn, J.; Wender, S.A. Neutron radiation hardness testing of 650V/7.5 A GaN power HEMT. *Radiat. Phys. Chem.* **2020**, *166*, 108456. [CrossRef]
169. Ngom, C.; Pouget, V.; Zerarka, M.; Coccetti, F.; Touboul, A.; Matmat, M.; Crepel, O.; Jonathas, S.; Bascoul, G. Backside Laser Testing of Single-Event Effects in GaN-on-Si Power HEMTs. *IEEE Trans. Nucl. Sci.* **2021**, *68*, 1642–1650. [CrossRef]
170. Hedayati, M.H.; Dymond, H.C.P.; Goswami, R.; Stark, B.H. Investigating GaN power device double-pulse testing efficacy in the face of VTH-shift, dynamic Rdson, and temperature variations. In Proceedings of the 2021 IEEE Applied Power Electronics Conference and Exposition (APEC), Phoenix, AZ, USA, 14–17 June 2021; pp. 2291–2298.
171. Van Do, T.; Trovao, J.P.F.; Li, K.; Boulon, L. Wide-Bandgap Power Semiconductors for Electric Vehicle Systems: Challenges and Trends. *IEEE Veh. Technol. Mag.* **2021**, *16*, 89–98. [CrossRef]
172. Dai, X.; Wang, Y.; Wu, Y.; Luo, H.; Liu, G.; Li, D.; Jones, S. Reliability design of direct liquid cooled power semiconductor module for hybrid and electric vehicles. *Microelectron. Reliab.* **2016**, *64*, 474–478. [CrossRef]
173. Li, J.; Zhang, H. Thermal characteristics of power battery module with composite phase change material and external liquid cooling. *Int. J. Heat Mass Transf.* **2020**, *156*, 119820. [CrossRef]
174. Bhalla, A.; Nava, M.; Zhu, M.; Sudario, F.; Sumaoang, D.; Alexandrov, P.; Li, X.; Losee, P. Ultra-high speed 7mohm, 650V SiC half-bridge module with robust short circuit capability for EV inverters. In Proceedings of the 2019 31st International Symposium on Power Semiconductor Devices and ICs (ISPSD), Shanghai, China, 19–23 May 2019; pp. 191–194.
175. Guan, Y.; Wang, Y.; Wang, W.; Xu, D. Analysis and Design of a 1-MHz Single-Switch DC–DC Converter with Small Winding Resistance. *IEEE Trans. Ind. Electron.* **2018**, *65*, 7805–7817. [CrossRef]

176. Knabben, G.C.; Schäfer, J.; Peluso, L.; Kolar, J.W.; Kasper, M.J.; Deboy, G. New PCB Winding "Snake-Core" Matrix Transformer for Ultra-Compact Wide DC Input Voltage Range Hybrid B+DCM Resonant Server Power Supply. In Proceedings of the 2018 IEEE International Power Electronics and Application Conference and Exposition (PEAC), Shenzhen, China, 4–7 November 2018; pp. 1–6.
177. Krismer, F.; Round, S.; Kolar, J.W. Performance optimization of a high current dual active bridge with a wide operating voltage range. In Proceedings of the 2006 37th IEEE Power Electronics Specialists Conference, Jeju, Republic of Korea, 18–22 June 2006; pp. 1–7.
178. Concari, L.; Barater, D.; Toscani, A.; Concari, C.; Franceschini, G.; Buticchi, G.; Liserre, M.; Zhang, H. Assessment of Efficiency and Reliability of Wide Band-Gap Based H8 Inverter in Electric Vehicle Applications. *Energies* **2019**, *12*, 1922. [CrossRef]
179. Wang, Y.; Ding, Y.; Yin, Y. Reliability of Wide Band Gap Power Electronic Semiconductor and Packaging: A Review. *Energies* **2022**, *15*, 6670. [CrossRef]
180. Huang, A.Q.; Zhu, Q.; Wang, L.; Zhang, L. 15 kV SiC MOSFET: An enabling technology for medium voltage solid state transformers. *CPSS Trans. Power Electron. Appl.* **2017**, *2*, 118–130. [CrossRef]
181. Wang, J.; Veliadis, V.; Zhang, J.; Alsmadi, Y.; Wilson, P.R.; Scott, M.J. IEEE ITRW Working Group Position Paper-System Integration and Application: Silicon Carbide: A Roadmap for Silicon Carbide Adoption in Power Conversion Applications. *IEEE Power Electron. Mag.* **2018**, *5*, 40–44. [CrossRef]
182. Pengelly, R.S.; Wood, S.M.; Milligan, J.W.; Sheppard, S.T.; Pribble, W.L. A Review of GaN on SiC High Electron-Mobility Power Transistors and MMICs. *IEEE Trans. Microw. Theory Tech.* **2012**, *60*, 1764–1783. [CrossRef]
183. Millan, J.; Godignon, P.; Perpina, X.; Perez-Tomas, A.; Rebollo, J. A Survey of Wide Bandgap Power Semiconductor Devices. *IEEE Trans. Power Electron.* **2014**, *29*, 2155–2163. [CrossRef]
184. ROHM Semiconductor. *SiC Power Devices and Modules Rev. 003*; Application Report; ROHM: Kyoto, Japan, 2020.
185. Bindra, A. Wide-Bandgap-Based Power Devices: Reshaping the power electronics landscape. *IEEE Power Electron. Mag.* **2015**, *2*, 42–47. [CrossRef]
186. Lumbreras, D.; Zaragoza, J.; Mon, J.; Galvez, E.; Collado, A. Efficiency analysis of wide band-gap semiconductors for two-level and three-level power converters. In Proceedings of the IECON 2019—45th Annual Conference of the IEEE Industrial Electronics Society, Lisbon, Portugal, 14–17 October 2019; pp. 5126–5133.
187. Scott, M.J.; Fu, L.; Zhang, X.; Li, J.; Yao, C.; Sievers, M.; Wang, J. Merits of gallium nitride based power conversion. *Semicond. Sci. Technol.* **2013**, *28*, 074013. [CrossRef]
188. Beheshti, M. Wide-Bandgap Semiconductors: Performance and Benefits of GaN Versus SiC. 2020. Available online: https://www.ti.com/lit/an/slyt801/slyt801.pdf?ts=1741160652383&ref_url=https%253A%252F%252Fwww.google.com%252F (accessed on 1 December 2024).